https://doi.org/10.5194/acp-2022-772
Preprint. Discussion started: 17 November 2022

Atmospheric Chemistry and Physics Discussions

Satellite measurements of plumes from the 2021 eruption of La Soufrière, St Vincent

Isabelle A. Taylor[1], Roy G. Grainger[1], Andrew T. Prata[2], Simon R. Proud[3,4], Tamsin A. Mather[5], and David M. Pyle[5]

[1]COMET, Sub-department of Atmospheric, Oceanic and Planetary Physics, University of Oxford, Oxford, OX1 3PU, UK
[2]Sub-department of Atmospheric, Oceanic and Planetary Physics, University of Oxford, Oxford, OX1 3PU, UK
[3]NCEO, Sub-department of Atmospheric, Oceanic and Planetary Physics, University of Oxford, Oxford, OX1 3PU, UK
[4]NCEO, RAL Space, STFC Rutherford Appleton Laboratory, Harwell, OX11, UK.
[5]COMET, Department of Earth Sciences, University of Oxford, Oxford, OX1 3AN, UK

Correspondence: Isabelle A. Taylor (isabelle.taylor@physics.ox.ac.uk)

Abstract. Satellite instruments play a valuable role in detecting, monitoring and characterising emissions of ash and gas into the atmosphere during volcanic eruptions. Plumes of ash and sulfur dioxide (SO_2) from the April 2021 eruption of La Soufrière volcano on St Vincent in the Eastern Caribbean were observed by a multiple satellite instruments. This study looks at these plumes with two satellite instruments: the Advanced Baseline Imager (ABI) on the Geostationary Operational Environmental Satellite (GOES), and the Infrared Atmospheric Sounding Interferometer (IASI) on the MetOp platforms. Using true and false colour images, and brightness temperature difference images produced from the ABI data, a minimum of 32 eruptive events were identified. The ABI images were used to determine the approximate start and end times and character of each event. In this way the eruption has been divided into four phases: (1) an initial explosive event, (2) a sustained event lasting over nine hours, (3) a pulsatory phase with 23 explosive events in a 54 hour period and (4) a waning sequence of explosive events. The IASI instrument was used to study the dispersion of SO_2 from this eruption. The results showed a highly complex structure to the plume, in terms of the column amounts and height, which is likely linked to the multiple explosive events. The SO_2 is shown to have largely been emitted between 13 and 19 km. This was primarily in the upper troposphere and around the height of the tropopause, but with some emission into the stratosphere. The SO_2 was transported around the globe with parts of the plume reaching as far as 45° S and 45° N. The largest SO_2 atmospheric burden measured with IASI was 0.31 ± 0.09 Tg, recorded on the 13 April 2021 (descending orbits). The SO_2 masses were converted into fluxes. The SO_2 flux was shown to peak on 10 April and then shown to decrease over time. By summing the IASI SO_2 flux results, it is estimated that a total of 0.57 ± 0.44 Tg of SO_2 was emitted to the atmosphere. However, due to the limitations associated with the retrieval this should be considered a minimum estimate of the total mass of SO_2 emitted. An average e-folding time of 7.09 ± 5.70 days was computed based on the IASI SO_2 results: similar to other tropical eruptions of this magnitude. There are a number of similarities between the 1979 and 2021 eruptions at La Soufrière. For example, both eruptions consisted of a series of explosive events with varied heights including some emission into the stratosphere. The similarities between the 1979 and 2021 highlight the importance of studying these eruptions to be prepared for future activity.

https://doi.org/10.5194/acp-2022-772
Preprint. Discussion started: 17 November 2022

Atmospheric Chemistry and Physics Discussions

1 Introduction

La Soufrière volcano (61.18° W, 13.33° N, summit elevation of 1220 m) located on the island of St Vincent in the Caribbean entered a phase of explosive activity on 9 April 2021 after having been in a lower level state of eruption, including the slow extrusion of a lava dome, since late December 2020 (Global Volcanism Program, 2021a; Joseph et al., 2022). The volcano is part of the Eastern Caribbean volcanic arc and has erupted on at least five occasions since the 18^{th} century in both explosive (1718, 1812, 1902-3, 1979) and lava dome-forming eruptions (1971-2, 1979) (Robertson, 1995; Pyle, 2017).

Eruptive activity since 1970 included the non-explosive extrusion of a basaltic andesite lava dome into the flooded crater from November 1971 - January 1972; and a violent series of explosions that began in the flooded summit crater on 13 April 1979 (Aspinall et al., 1973; Shepherd et al., 1979). The 1979 explosions were very well documented at the time and persisted for two weeks. They were followed by about six months of lava dome extrusion across the crater floor, which by then had been infilled by pyroclastic ejecta (Brazier et al., 1982; Fiske and Sigurdsson, 1982; Shepherd and Sigurdsson, 1982). The explosive eruption of La Soufrière in April 1979 was one of the first eruptions to have occurred during the "satellite era" (Fiske and Sigurdsson, 1982). Observations from the infra-red radiometer on the geostationary satellite SMS-1 were used to measure the growth of the volcanic ash plumes (Krueger, 1982); early measurements from the Stratospheric Aerosol and Gas Experiment (SAGE) detected stratospheric aerosol following the eruption (McCormick et al., 1982); and SO_2 from the eruption was detected by the Total Ozone Mapping Spectrometer (TOMS; Carn et al. 2003, 2016).

After the 1979 eruption, La Soufrière showed no detectable signs of activity or unrest until late 2020. An increase in seismicity was noted by seismologists at The University of the West Indies Seismic Research Centre (UWI-SRC) in November and December 2020 (Joseph et al., 2022). An effusive eruption began on 27 December 2020 with the emplacement of a new lava dome, which grew over the following months. On 8 April 2021, the alert level was raised to the highest level and an evacuation of the highest risk communities was ordered (Global Volcanism Program, 2021b). The first of a number of explosive eruptive events began on 9 April 2021 at 08:41 LT (12:41 UTC) (Joseph et al., 2022). Multiple explosive events occurred over the following two weeks, with the last explosive event occurring on 22 April 2021. Activity during this eruptive period led to the closure of local airports and ash fall affected much of St Vincent, as well as neighbouring islands including the Grenadines, Barbados and Saint Lucia (Global Volcanism Program, 2021b).

Advances in satellite technology in the last four decades mean that in 2021 multiple aspects of the volcano's activity including thermal anomalies, dome growth, lightning and the evolution of the SO_2 and ash plumes, were studied with satellite instruments (Global Volcanism Program, 2021a, b; Smart and Sales, 2021; Ravindra Babu et al., 2022; Thompson et al., 2022; Yue et al., 2022; Horváth et al., 2022). Measurements made by satellite instruments allow the detection of SO_2 and ash, and quantification of the plume properties. This is essential for assessing the potential hazard of volcanic plumes to aircraft (Prata and Tupper, 2009; Thomas and Watson, 2010; Lechner et al., 2017) and providing estimates of the eruption source parameters

https://doi.org/10.5194/acp-2022-772
Preprint. Discussion started: 17 November 2022


Atmospheric Chemistry and Physics Discussions

(Aubry et al., 2021). Of particular value is the ability of satellite instruments to track the evolution of these plumes as they are transported away from the source.

This paper uses data from the Infrared Atmospheric Sounding Interferometer (IASI) on the MetOp satellites, and the Advanced Baseline Imager (ABI) on the Geostationary Operational Environmental Satellite (GOES) to study the plumes of ash and SO_2 from the 2021 eruptions of La Soufrière. Further details on the instruments and methods used to retrieve information about the plumes are given in section 2. The eruption sequence and plume characteristics are discussed in section 3. These instruments provide a complementary view of the eruption with the high temporal resolution of ABI allowing the eruption sequence to be evaluated, while using IASI it possible to study the dispersion of the plumes as they travel across the globe.

2 Methods

2.1 The Infrared Atmospheric Sounding Interferometer

2.1.1 Instrument

The Infrared Atmospheric Sounding Interferometer (IASI) is a Fourier transform spectrometer on-board three meteorological satellite instruments: MetOp-A, -B and -C launched in 2006, 2012 and 2018 respectively. The instrument's field-of-view consists of four circular pixels each with a 12 km diameter (at nadir) within a 50 by 50 km square at nadir (Clerbaux et al., 2009). The instruments measure across a wide spectral range within the infrared part of the electromagnetic spectrum between 645 and 2760 cm^{-1} (3.6 - 15.5 μm) with a high spectral sampling of 0.25 cm^{-1} and apodized spectral resolution of 0.5 cm^{-1} (Blumstein et al., 2004). More information on the IASI instrument can be found in Clerbaux et al. (2009). Within the instrument's spectral range there is sensitivity to volcanic ash (v-shaped absorption feature between 750 and 1250 cm^{-1}; Clarisse et al. 2010a) and SO_2 (three absorption features ν_1, ν_3 and ν_1+ν_3, centred at 8.7, 7.3 and 4 μm respectively). A number of methods have been developed to extract information about SO_2 from the IASI spectra (e.g. Clarisse et al., 2008; Walker et al., 2011; Clarisse et al., 2012; Carboni et al., 2012; Walker et al., 2012; Clarisse et al., 2014). Retrieval techniques have been developed to obtain information about other volcanic gas species including H_2S (Clarisse et al., 2011) and CO (Martínez-Alonso et al., 2012). Additional work has been done on the retrieval of sulfate (Guermazi et al., 2021) and ash particles (Clarisse et al., 2010a, b; Maes et al., 2016; Ventress et al., 2016; Taylor et al., 2019). Each IASI instrument obtains near global coverage twice a day and there is no break in coverage associated with the loss of solar radiation at night and during high latitude winters. This coverage and sensitivity to gases and aerosols associated with volcanic eruptions makes the IASI instruments well-suited for studying the evolution of volcanic plumes. This study uses retrieval schemes developed by Walker et al. (2011, 2012) and Carboni et al. (2012) for quantifying SO_2 emissions from La Soufrière and Sears et al. (2013) for the detection of volcanic ash.

https://doi.org/10.5194/acp-2022-772
Preprint. Discussion started: 17 November 2022


Atmospheric Chemistry and Physics Discussions

2.1.2 Retrievals

In this study, two methods have been employed for studying the SO_2 plumes from the La Soufrière eruption. The first method is a linear retrieval which is applied in this case to detect pixels which contain elevated quantities of SO_2. Full details of this method can be found in Walker et al. (2011, 2012). The second method is an optimal estimation retrieval scheme which is able to quantify information about the plume including the column amount, height and the effective radiating temperature, and the errors associated with each of these. In this study it has been applied to pixels flagged by the linear retrieval as containing SO_2. The retrieval has been run in much the same way as is described in Carboni et al. (2012, 2016, 2019). However, there are a few notable differences:

- A higher *a priori* height has been used. In most previous applications, an *a priori* height of 400 hPa (∼7.6 km) has been used. This has been changed to 150 hPa (∼14.3 km; upper troposphere) to reflect the higher injection height of the La Soufrière eruption as reported in Global Volcanism Program (2021b). The *a priori* variance has been kept at 500 hPa.
- In previous applications of the retrieval, the 1σ plume thickness was constrained and set to 100 hPa. This is more appropriate for a plume in the lower troposphere (∼1.9 km at 400 hPa), but due to the exponential change in pressure with height in the atmosphere, this thickness is inappropriate in the upper troposphere and lower-stratosphere (UTLS) (∼4.8 km at 150 hPa). In this application the *a priori* plume thickness has been set to 30 hPa (∼1.2 km at 150 hPa): this is the minimum thickness that can be set given the spacing of the RTTOV (the forward model used) pressure levels. Changing the thickness highlights a potential area for future work: developing a new version of the retrieval which works in height in kilometers or log pressure so that a constant thickness can be set.

As in Carboni et al. (2012), a quality control is applied to the results. This requires that the retrieved values have column amounts exceeding 0 DU, retrieved pressures of between 0 and 1100 hPa, heights greater than 0 km, a cost value of less than 10, and that the retrieval converged within 10 iterations.

To estimate the total mass of SO_2 the retrieved column amounts are first gridded to a regular grid of 0.125 by 0.125°(roughly 13.5 by 13.91 km at 13° N, 61° W): the retrieved values are interpolated to fill gaps created by the IASI field-of-view and where pixels fail the quality control. Using the area of each grid box, the column amount are converted to a mass and the total mass is then computed by summing all the gridded masses within a defined region (-45 to 45° N and -180 and 180° E). Similarly, a vertical distribution of the SO_2 mass can be obtained by combining the mass grid with a height grid generated from the retrieved heights.

Error analysis by Carboni et al. (2012) explored the effects of cloud and volcanic ash on the iterative SO_2 retrieval. This analysis demonstrated that ash with an optical depth of 1 (at 550 nm) can significantly effect the output of the retrieval. An ash optical depth of 2 was shown to cause a 50 % underestimation in the SO_2 column amount, and an optical depth of 5 was shown to mask the SO_2 signal completely. To investigate the effect of ash on the La Soufrière results, a linear ash retrieval as described in Sears et al. (2013) has been applied to the IASI data to detect pixels containing volcanic ash which may affect the retrieved SO_2 values. This retrieval is run at three pressure levels (400, 600 and 800 hPa) to obtain three estimates of the

https://doi.org/10.5194/acp-2022-772
Preprint. Discussion started: 17 November 2022

Atmospheric Chemistry and Physics Discussions

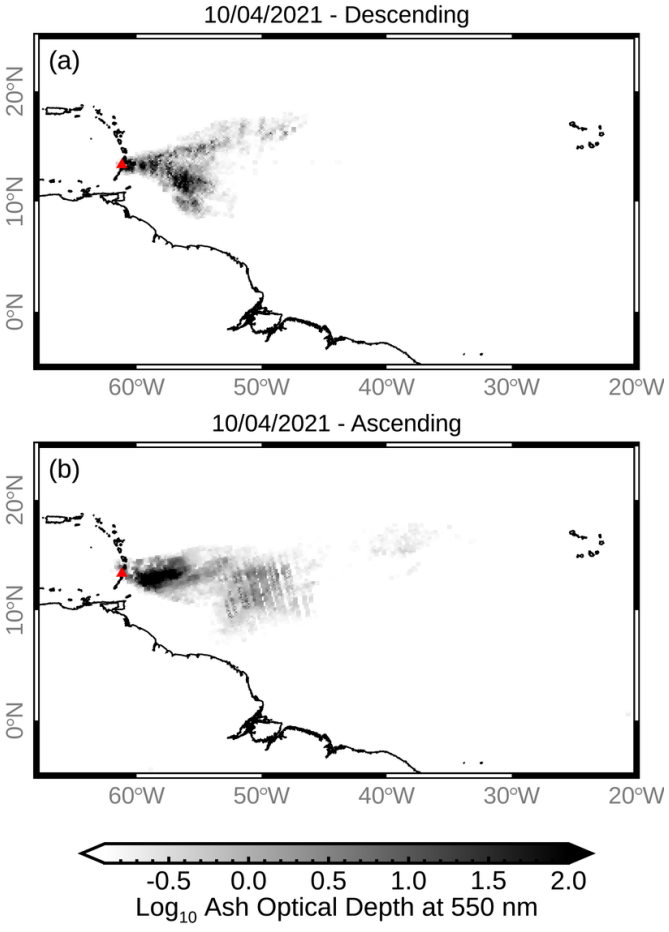

Figure 1. Ash optical depths at 550 nm from the IASI linear ash retrieval for 10 April 2021. This retrieval was run assuming a height of 400 hPa. The volcano's location is indicated by a red triangle.

optical depth. Pixels are then flagged as containing volcanic ash if they exceed a threshold for any of the heights. In this study, the results for the 400 hPa (∼7.6 km) level are used as it is the closest level to the retrieved heights.

Figure 1 shows an example of the linear ash retrieval on 10 April 2021. The retrievals show a optically thick ash plume travelling east from the volcano. It is therefore likely that the retrieved SO_2 column amounts for this observation time are affected by ash. Table 1 indicates the percentage of SO_2 flagged pixels on 10-11 April where the ash optical depths are greater than 1, 2 and 5. Note that to avoid false detection over the Sahara (due to the surface emissivity), the ash linear retrieval has been run for a smaller region (5° S to 25° N, -68 to -20° E) than the main analysis. The percentage of SO_2 flagged pixels affected by ash peaks on 10 April 2021 (descending orbits; local overpass time at the tropics is around 9:30) of which 15.8 % 11.6 % and 7.7 % have ash optical depths of greater than 1, 2 and 5 respectively. This analysis gives some indication of the

https://doi.org/10.5194/acp-2022-772
Preprint. Discussion started: 17 November 2022

Atmospheric Chemistry and Physics Discussions

Table 1. Percentage of IASI SO_2 pixels on 10 and 11 April 2021 which may be affected by volcanic ash. This has been calculated for the region 5° S to 25° N, -68 to -20° E.

Date (dd/mm/yyyy) and orbit direction	Number of pixels containing SO_2	% SO_2 flagged pixels containing ash with AOD $\geq$ 1	% SO_2 flagged pixels containing ash with AOD $\geq$ 2	% SO_2 flagged pixels containing ash with AOD $\geq$ 5
10/04/2021 Descending	3645	15.8	11.6	7.7
10/04/2021 Ascending	4482	10.5	7.2	4.1
11/04/2021 Descending	4742	3.1	1.8	1.1
11/04/2021 Ascending	3767	0.2	0.02	0

impact of ash on the retrieval results, and so the column amount and mass values presented in this paper should be considered to be minimum estimates. Future work should consider the simultaneous retrieval of ash and SO_2 so as to reduce the impact of ash on the SO_2 iterative retrieval. Additionally, SO_2 may be missed where it falls below the retrieval detection limit.

2.1.3 Estimating SO_2 e-folding time and flux

The decrease in the total mass of SO_2 (m) in the atmosphere with time (t) can be described as:

$$\frac{dm}{dt} = -\frac{1}{\lambda}m \tag{1}$$

Where λ is the average SO_2 e-folding time. Fitting Eq. 1 to the total SO_2 atmospheric burden obtained with a satellite instrument can give a simple estimate of the e-folding time. However, this approach neglects the variable flux of SO_2 emitted from the volcano. An optimal estimation scheme developed by Carboni et al. (2019) considers that the total SO_2 value is effected by both the e-folding time and variable SO_2 flux (f):

$$m_i = m_{i-1}e^{-\frac{1}{\lambda}\Delta t} + f\lambda(1 - e^{-\frac{1}{\lambda}\Delta t}) \tag{2}$$

Where i is the time step and Δt is the time interval between measurements.

The Carboni et al. (2012) approach was applied to the IASI total SO_2 mass values obtained for La Soufrière to obtain estimates of the flux at each time step and an average e-folding time. It was noted that in this case the average e-folding estimate was strongly influenced by the *a priori* value. Subsequently, an independent estimate of the e-folding time was computed by fitting Eq. 1 to the IASI SO_2 masses computed for the 23-28 April 2021 (the period after the last explosive event occurred). This is shown in Fig. 2 and produced an e-folding estimate of 6.61 days. This value was used as the *a priori* in the optimal estimation approach to getting flux and e-folding time for the 9 to 22 April 2021. The optimal estimation scheme produced an e-folding time of 7.09 ± 5.7 days. On days with no explosive events, as identified with the ABI data, the *a priori* SO_2 flux and uncertainty are set to 0. The event start and end times obtained from the ABI data were used to inform this.

https://doi.org/10.5194/acp-2022-772
Preprint. Discussion started: 17 November 2022

Atmospheric Chemistry and Physics Discussions

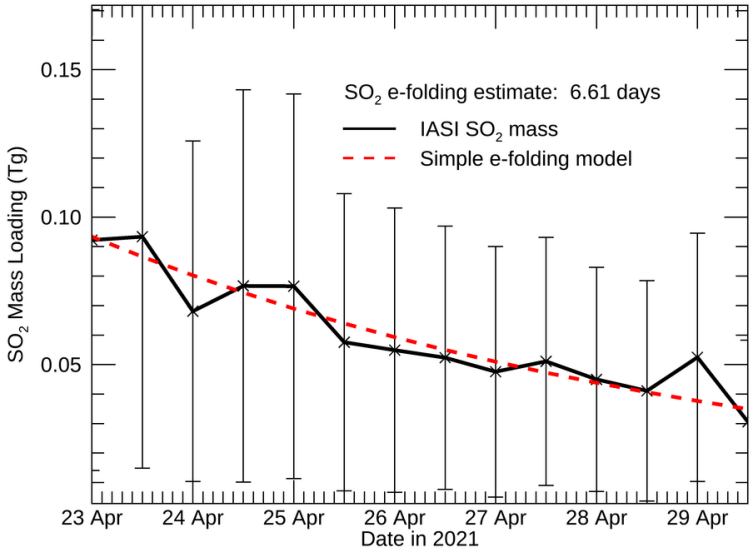

Figure 2. IASI SO_2 masses for 23-28 April 2021: the period after the last eruptive event at La Soufrière. A simple and independent estimate of SO_2 e-folding time has been computed by fitting Eq. 1 to the IASI total SO_2 mass estimates. This has been used as an independent *a priori* in the optimal estimation method for obtaining the flux and average e-folding time for the eruptive period (9-22 April).

To compute the total mass of SO_2 erupted over the studied period, the fluxes were summed and then multiplied by the time difference (Δt) between the descending and ascending orbits (assumed to be 12 hours). Any negative fluxes were excluded from this calculation. To estimate the total erupted mass error, the individual flux errors are summed in quadrature, and then multiplied by Δt. An alternative estimate of the maximum total erupted mass value has been obtained by summing the SO_2 fluxes added to the errors and then multiplying by Δt. A minimum value is obtained in the same way but this time subtracting the errors (negative values are excluded).

2.2 The Advanced Baseline Imager (ABI)

2.2.1 Instrument

The Advanced Baseline Imager (ABI) is on-board three of the Geostationary Operational Environmental Satellite platforms: GOES-16 (or GOES-East), GOES-17 (or GOES-West) and GOES-18 launched in 2016, 2018 and 2022 respectively. The GOES-16 instrument is used in this study. The area imaged by GOES-16 (positioned at 75.2° W) covers most of the continental United States, Eastern Canada, Central and South America and the Caribbean. In addition it covers the Eastern Pacific and a large part of the Atlantic Ocean. The ABI instrument has sixteen channels spanning the 0.45 to 13.7 μm spectral range, with

https://doi.org/10.5194/acp-2022-772
Preprint. Discussion started: 17 November 2022


Atmospheric Chemistry and Physics Discussions

the spatial resolution for the different channels varying from 0.5 to 2 km at nadir (Schmit et al., 2005). Seven channels between 7.3 and 13.3 μm mean that the instrument has sensitivity to ash and SO_2, and the instrument has previously been used for the detection of ash and SO_2, and quantification of ash properties (e.g. Pavolonis et al., 2020). Previous versions of the ABI instruments have also been used for this purpose (e.g. Yu et al., 2002; Ackerman et al., 2008). During the eruption of La Soufrière, the ABI sensor recorded a new full disc image every 10 minutes. In addition, on GOES-16 there are two moveable mesoscale regions which provide data every minute. During the La Soufrière eruption, one mesoscale region was moved over the volcano. This started at 9:00 UTC on 10 April (missing the earlier eruptive events) and ended at 06:00 UTC on 16 April 2021 (before the last three eruptive event). In this study, the ABI data has been used to identify the start and end times of each eruptive event, and for determining the height of the ash cloud. When available the 1-minute mesoscale data have been used for the identification of the start and end times of the eruptive events. The 10-minute resolution data have been used for the remaining days. The 10-minute data has been used for the height analysis. While the ABI instrument has sensitivity to ash and SO_2 it has not been used to quantify the amount of either in this study. Instead it has been used to document the sequence of explosive events produced by the 2021 La Soufrière eruption.

2.2.2 Analysis of ash

True and false colour maps have been produced from the ABI data for the eruption period (9-22 April 2021). The false colour images have been constructed by assigning the 12.3 - 10.3 μm, 11.2 - 8.4 μm and 10.3 μm channels to red, green and blue respectively. In these maps the optically thick cloud (ice, ash or meteorological cloud) appears in shades of brown/orange, less optically thick volcanic ash appears in shades of red/pink and SO_2 appears bright green/blue. An example of these plots can be seen in Fig. 3. In addition, the 11.2 - 12.3 μm and 10.3 - 11.2 μm Brightness Temperature Differences (BTDs) have been calculated. The 11.2 - 12.3 BTD combination has been widely used to distinguish volcanic ash in satellite data and uses the positive transmission gradient between 10 and 12 μm caused by volcanic ash (Prata, 1989a, b). The 10.3 μm micron channel is less affected by water vapour (Lindsey et al., 2012) and so the 10.3-11.2 BTD may be more appropriate in tropical atmospheres. A threshold can be used to flag pixels containing ash. The BTD approach can be limited for a number of reasons, for example, false detections can occur in regions with high surface emissivities (e.g. deserts) and strong temperature inversions, or due to desert dust, while ash clouds may not be identified if they are too optically thin or thick, or if there are significant quantities of ice or water within the plume (Rose et al., 1995; Simpson et al., 2000; Prata et al., 2001). Also there is no generally applicable threshold which can be set for ash detection with the most appropriate value varying with region and time.

Together the true, false and BTD images have been used to study the evolution of the plumes from La Soufrière. Careful examination of the plots allowed the identification of the approximate start and end times of each eruptive event. This process also allowed some inference of the character of each event. This analysis is limited by the 10/1-minute resolution of the ABI instrument and can be complicated by the presence of cloud. The interpretation of the end time was particularly challenging and somewhat subjective. In general, the end time was determined when the plume moved away from the volcano. This can be affected by the wind speed and so the end times should be considered approximate. It is also possible that lower level eruptive activity may not be identifiable in the ABI data. Note that for the full disc the measurement time over La Soufrière has been

https://doi.org/10.5194/acp-2022-772
Preprint. Discussion started: 17 November 2022

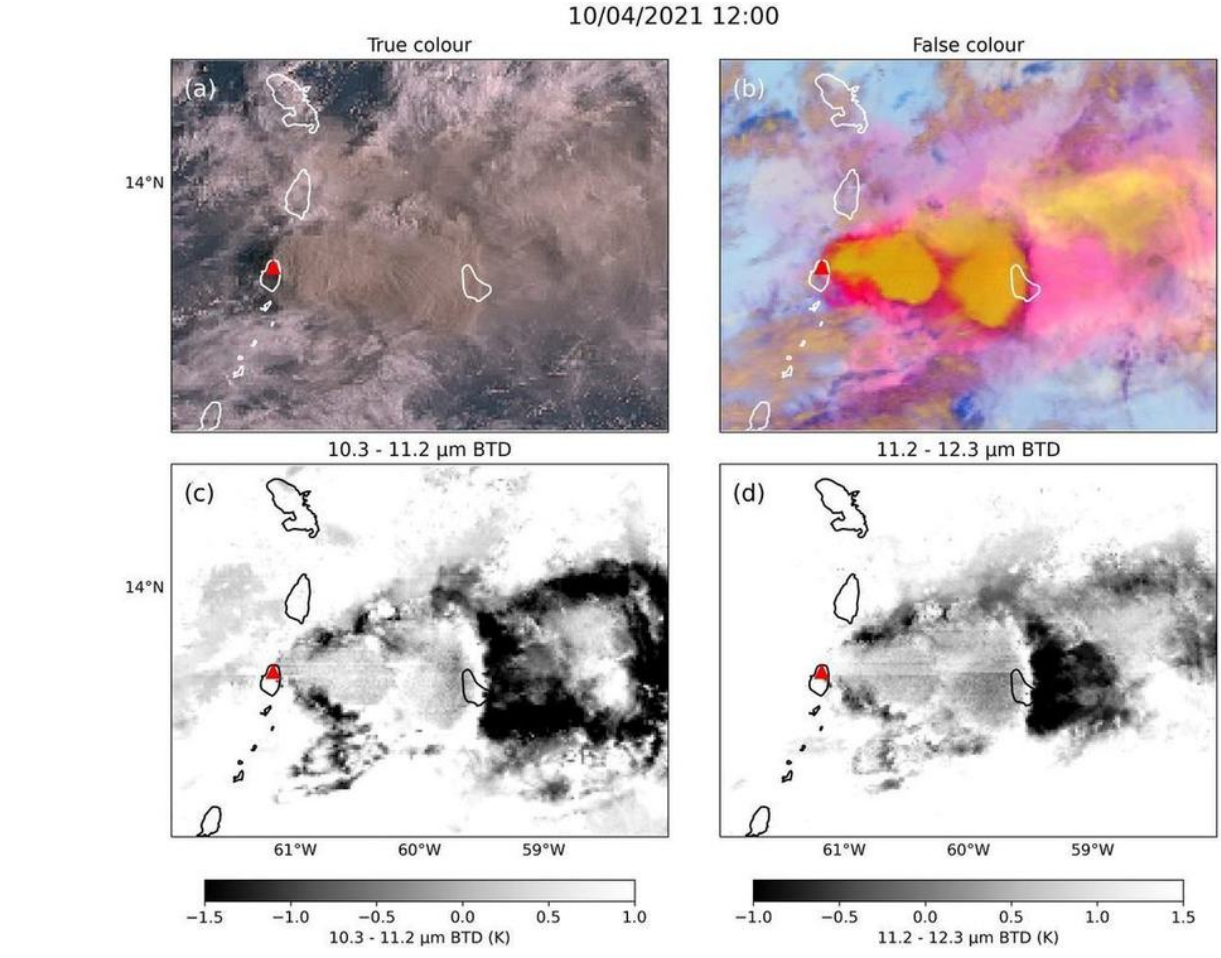

Figure 3. Examples of results from the ABI instrument for the La Soufrière plume at 12:00 on 10 April 2021 . (a) True colour image. (b) False colour image (12.3 - 10.3 μm, 11.2 - 8.4 μm and 10.3 μm channels assigned to red, green and blue respectively). (c) 10.3 - 11.2 μm BTD. (d) 11.2 - 12.3 μm BTD. Plots for the period studied can be found in the supplementary information.

computed based on the latitude of the volcano and the rough measurement start and end times. This is estimated to be roughly 243 seconds (4 minutes and 3 seconds) from the start time. This has been used to report the times for the full disc results in this study. No such adjustment has been made to the mesoscale results where the measurement start time has been used.

An estimate of the ash height is obtained by comparing the brightness temperature in the 11.2 μm band (ABI channel 14) for each eruptive event in a 0.1 degree box around the volcano with the ERA-5 ECMWF temperature profile interpolated to the volcano's location (European Centre for Medium-Range Weather Forecasts, 2021). This method will be now be referred to as the "Brightness Temperature (BT) method". The measured brightness temperature is representative of the temperature at the top of the ash or cloud layer. The 11.2 μm channel is within an atmospheric window that has little sensitivity to water vapour. The minimum (or coldest) value within the 0.1 degree box around the volcano helps to select the optically thickest

https://doi.org/10.5194/acp-2022-772
Preprint. Discussion started: 17 November 2022


Atmospheric Chemistry and Physics Discussions

part of the plume and therefore the pixel which is least likely to be affected by radiation from beneath the plume. The box size should remove any effect due to parallax. This method has been widely used to estimate the ash cloud top height (e.g. Prata and Grant, 2001). There are however a few limitations which are discussed in several papers (e.g. Oppenheimer, 1998; Prata and Grant, 2001; Zakšek et al., 2013). (1) In its application here, this method only returns a single height rather than reflecting the heights across the plume. In addition, in this study, the minimum BT has been selected for each eruptive event (referred to as the "optically thick height method/solution") and so the reported values do not reflect the variation in height during the eruptive event. (2) A good quality temperature profile, close to the volcano, is required. (3) When the plume is optically thin, upwelling radiation from beneath the plume contributes to the measured brightness temperature: an effect minimised here by selecting the pixel with the coldest brightness temperature. (4) The method assumes that the ash is at an equal temperature to the surrounding air, if this is not the case, then the method will not perform well. (5) Multiple solutions can arise due to multiple intersections with the temperature profiles (e.g. above and below the tropopause, and other temperature inversions), in such cases, additional data sources are required to clarify the result. In this study multiple solutions are reported. (6) The method can be limited in isothermal atmospheres (e.g. Prata et al., 2022). (7) It does not account for absorption above the cloud top. Despite the various limitations of this method, it is a quick and frequently used approach for estimating ash cloud heights. For this application an uncertainty of 1 K has been assumed for the instrument measurement encompassing the instrument noise and gaseous absorption above the cloud.

In this study, there was commonly a tropospheric and stratospheric solution when using the BT method. Additional information has been obtained by comparing the plume direction and speed with the ERA-5 ECMWF wind profiles. Figure 4a shows the average and standard deviation of the wind direction with height. The average wind speed with height is shown in Fig. 4b. At heights of less than 5 km the wind is primarily travelling to the west (e.g. 267.5°at 4.3 km) with wind speeds of less than 10 m s^{-1}. At around 5 km the wind direction shifts to the east. Between 7 and 17 km the wind direction is fairly consistent (varying between 101 and 126°) before shifting back to the west at 19 to 20 km. The wind speed is shown to increase between 5 and 14 km and then fall between 15 and 20 km. Figure 4c and d show the average plume direction and speed. This has been computed by visually identifying the centre of the optically thick plume in the RGB image, an hour, or 30 minutes, after the start of each eruptive event (as identified with ABI). For the first 6 days of the eruption, where there is some uncertainty with regard to the height, the plume is shown to broadly be travelling to the east: supporting a tropospheric solution. To take this analysis further, at the location identified as the centre of the optically thick plume, the BT method was used to obtain a second set of height solutions (referred to as the "BT method-centre" solutions). The wind directions at the heights obtained with both BT methods are compared against the plume vector components to assign a degree of confidence to the height results for each eruptive event. Figure 5 shows examples from the first three eruptive events which were shown to be tropospheric, uncertain and stratospheric respectively. There are differences between the heights obtained with the "BT method" applied in this study and the results obtained using the BT method and side angle height estimates found in Horváth et al. (2022). One possible reason for this is sampling different parts of the plume.

https://doi.org/10.5194/acp-2022-772
Preprint. Discussion started: 17 November 2022

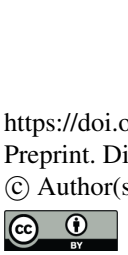

Atmospheric Chemistry and Physics Discussions

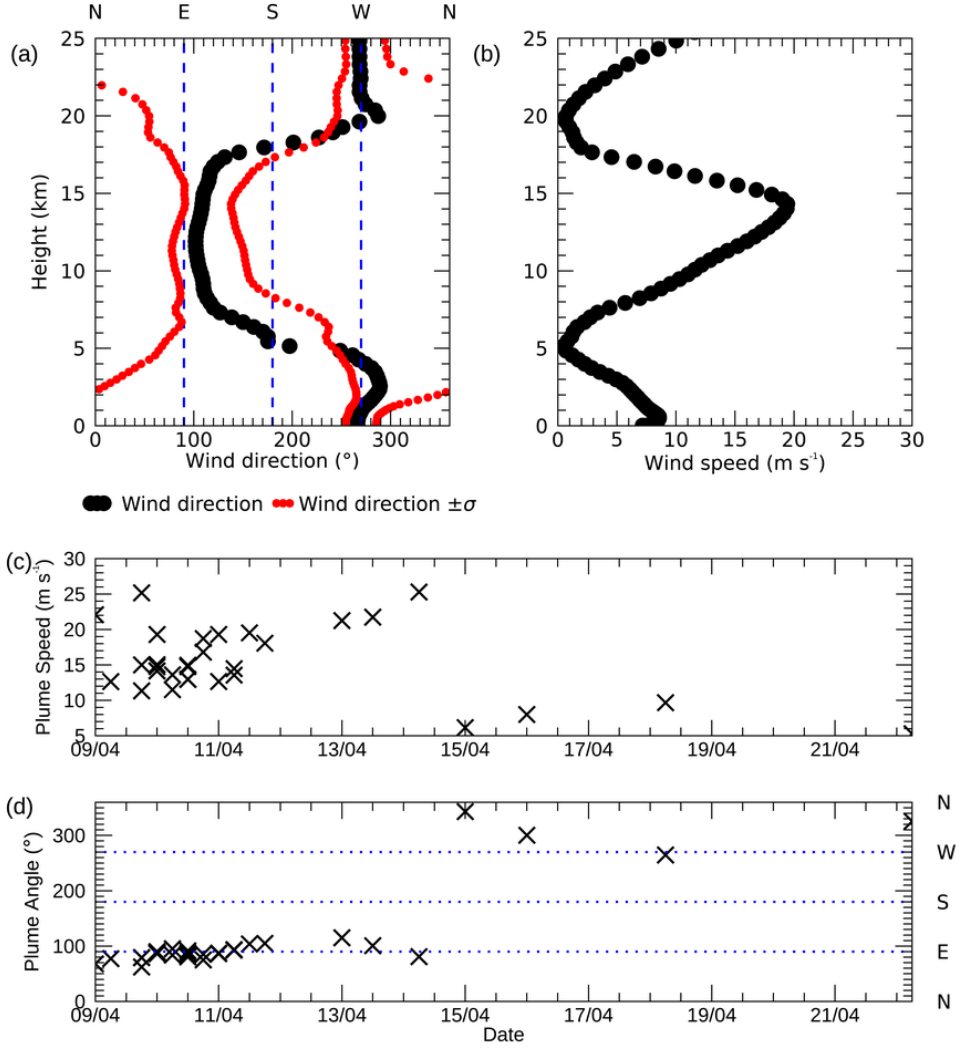

Figure 4. (a) The average and standard deviation of the ERA5 ECMWF wind direction for different height layers between 9 and 22 April. (b) Average wind direction profile of the ERA5 ECMWF wind direction for different height layers between 9 and 22 April. (c) Plume speed for the different explosive events. (d) Plume direction of travel for the different explosive events.

https://doi.org/10.5194/acp-2022-772
Preprint. Discussion started: 17 November 2022

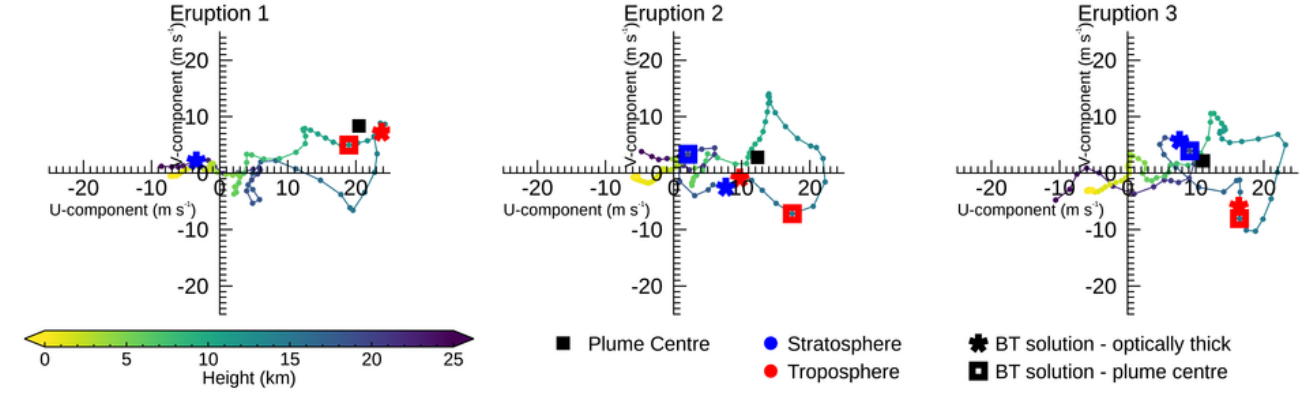

Figure 5. Demonstration of the use of the ERA5 ECMWF wind data to determine whether the tropospheric or stratospheric solution is more likely. Examples are from the first three eruptive events (see Table 2). These were classified as tropospheric, inconclusive and stratospheric respectively.

3 Results

3.1 Eruption sequence

True and false colour maps and ash BTDs were produced from the ABI data for the entire eruptive period (9-22 April 2021) using the instrument's high temporal resolution. An example from 10 April at 12:00 UTC is shown in Fig. 3. Animations showing the true and false colour images and the BTD maps for each eruptive event can be found at http://eodg.atm.ox.ac.uk/ABI/la_soufriere/ (EODG 2022; webpage last access on 8 November 2022). These images have been carefully examined to get start and end times for each of the explosive events identified. The start and end times are reported in Table 2. The heights obtained with the BT method are reported in Table 3.

Using the ABI data, a minimum of 32 explosive events containing volcanic ash were identified. The number identified is limited by the temporal resolution of the instrument and cloud cover that might obscure the plume, and so could potentially be higher. For example, explosive events that last less than 10 minutes may not be identified in the 10-minute resolution data, or discrete eruptions or pulses that occur within the 1 or 10 minutes between images may be classified as the same eruption. Times where this is suspected are mentioned in Table 2. Additionally, lower level activity may not be visible within the ABI data. Figure 6a shows the number of explosive events, determined with the ABI data, which started on each day. This is shown to be highest on the 10 April and decreases throughout the remainder of the eruptive sequence, with Fig. 6 showing that the repose time between explosive events increases over time. The duration of the eruptive events (Fig. 6c) is also shown to generally increase throughout the 9-22 April eruptive period as also noted by Joseph et al. (2022).

https://doi.org/10.5194/acp-2022-772
Preprint. Discussion started: 17 November 2022

Atmospheric Chemistry and Physics Discussions

Table 2. Summary of plumes from La Soufrière seen with the ABI satellite instrument. The start and end times have been determined with the ABI images. The eruption has been split into four phases based on the general character of the events.

Phase	Event number	Start Date (dd/mm/yyyy hh:mm UTC)	End Date (dd/mm/yyyy hh:mm UTC)	Notes
1: initial explosive event	1	09/04/21 12:54	09/04/21 15:54	Small plume travelling W. Main optically thick plume travelling ENE, after 13:14 becomes less optically thick. Thick cloud cover after 15:34 makes end time difficult to determine
2: sustained ash emission event	2	09/04/21 19:04	10/04/21 04:44	Large, sustained eruptive event with optically thick ash cloud. Shape of plume suggests possible strong pulses within this eruptive phase at around 19:24, 20:14, 21:14, 21:44, 22:24, 23:24 UTC on 9 April, and 03:34, 03:54 on 10 April. However, 10-minute temporal resolution does not allow these to be confirmed.
3: pulsatory phase	3	10/04/21 04:54	10/04/21 06:04	Beginning of shorter pulses. Optically thick ash with small gaps between
	4	10/04/21 07:04	10/04/21 07:34	Small emission to start followed by large optically thick plume.
	5	10/04/21 07:44	10/04/21 09:45	1-minute resolution data used here for first time in analysis (for the end time)
	6	10/04/21 09:46	10/04/21 10:54	
	7	10/04/21 10:55	10/04/21 12:09	
	8	10/04/21 12:10	10/04/21 13:01	
	9	10/04/21 13:02	10/04/21 14:36	
	10	10/04/21 14:37	10/04/21 16:23	
	11	10/04/21 16:24	10/04/21 18:47	
	12	10/04/21 18:48	10/04/21 21:25	
	13	10/04/21 21:26	10/04/21 23:07	
	14	10/04/21 23:08	11/04/21 00:37	
	15	11/04/21 01:02	11/04/21 02:14	
	16	11/04/21 02:50	11/04/21 04:23	
	17	11/04/21 05:06	11/04/21 05:43	
	18	11/04/21 08:03	11/04/21 09:47	Initially optically thick ash cloud becoming optically thin.
	19	11/04/21 10:43	11/04/21 11:51	
	20	11/04/21 13:32	11/04/21 18:13	Initially optically thick ash cloud becoming optically thinner. Difficult to distinguish end time

https://doi.org/10.5194/acp-2022-772
Preprint. Discussion started: 17 November 2022

Atmospheric Chemistry and Physics Discussions

Table 2. Continued

Phase	Event number	Start Date (dd/mm/yyyy hh:mm UTC)	End Date (dd/mm/yyyy hh:mm UTC)	Notes
	21	11/04/21 18:14	11/04/21 20:07	Initially optically thick ash cloud becoming optically thinner. Difficult to distinguish end time
	22	11/04/21 20:08	11/04/21 23:44	Initially optically thick ash cloud becoming optically thinner over time
	23	12/04/21 00:10	12/04/21 00:25	Very small plume to the E
	24	12/04/21 00:47	12/04/21 02:26	Initially optically thick ash cloud becoming optically thinner over time. Hard to distinguish the end time
	25	12/04/21 08:06	12/04/21 10:16	Initially optically thick ash cloud becoming optically thinner over time. Difficult to distinguish the end time
4: waning stage	26	13/04/21 10:36	13/04/21 14:15	Initially optically thick ash cloud becoming optically thin over time. Difficult to distinguish the end time
	27	14/04/21 02:35	14/04/21 06:40	Emission of optically thin ash before (starting 01:45 travelling to the N)
	28	14/04/21 15:42	14/04/21 17:45	Initially optically thick ash cloud becoming optically thinner
	29	15/04/21 09:06	15/04/21 10:24	Last use of 1-minute resolution data
	30	16/04/21 10:24	16/04/21 17:04	Optically thinner plume visible amongst light cloud layers
	31	18/04/21 20:54	19/04/21 00:14	Optically thin plume
	32	22/04/21 15:24	22/04/21 21:54	Optically thin plume

https://doi.org/10.5194/acp-2022-772
Preprint. Discussion started: 17 November 2022

Atmospheric Chemistry and Physics Discussions

Table 3. Heights retrieved using BT method applied to ABI data.

	Optically thick height solution (km)		Plume centre height solution (km)	
Event number	**Troposphere**	**Stratosphere**	**Troposphere**	**Stratosphere**
1	$13.11^{+0.12}_{-0.12}$	$22.77^{+0.23}_{-0.26}$	$11.98^{+0.13}_{-0.16}$	
2	$16.78^{+0.24}_{-0.20}$	$17.45^{+0.11}_{-0.11}$	$15.21^{+0.19}_{-0.29}$	$19.28^{+0.14}_{-0.15}$
3	$15.80^{+0.16}_{-0.18}$	$18.89^{+0.14}_{-0.19}$	$15.48^{+0.18}_{-0.20}$	$19.20^{+0.16}_{-0.14}$
4	$12.96^{+0.11}_{-0.11}$	$21.91^{+0.19}_{-0.15}$	$12.42^{+0.13}_{-0.13}$	$23.65^{+1.20}_{-0.92}$
5	$14.85^{+0.14}_{-0.15}$	$20.01^{+0.14}_{-0.17}$	$13.25^{+0.10}_{-0.10}$	$21.36^{+0.16}_{-0.15}$
6	$15.34^{+0.18}_{-0.16}$	$19.16^{+0.19}_{-0.16}$	$15.40^{+0.20}_{-0.18}$	$19.10^{+0.18}_{-0.16}$
7	$15.58^{+0.24}_{-0.19}$	$18.95^{+0.16}_{-0.16}$	$15.40^{+0.19}_{-0.16}$	$19.10^{+0.16}_{-0.16}$
8	$15.94^{+0.19}_{-0.22}$	$18.71^{+0.15}_{-0.15}$	$15.34^{+0.16}_{-0.15}$	$19.17^{+0.13}_{-0.16}$
9	$15.15^{+0.16}_{-0.15}$	$19.30^{+0.09}_{-0.09}$	$15.77^{+0.19}_{-0.24}$	$18.89^{+0.15}_{-0.13}$
10	$14.85^{+0.16}_{-0.15}$	$19.38^{+0.10}_{-0.10}$	$15.60^{+0.22}_{-0.21}$	$18.93^{+0.12}_{-0.12}$
11	$15.11^{+0.26}_{-0.21}$	$19.19^{+0.15}_{-0.18}$	$15.01^{+0.18}_{-0.16}$	$19.24^{+0.12}_{-0.14}$
12	$14.35^{+0.15}_{-0.12}$	$19.91^{+0.23}_{-0.21}$	$14.56^{+0.21}_{-0.15}$	$19.61^{+0.21}_{-0.17}$
13	$16.16^{+0.12}_{-0.13}$	$18.44^{+0.17}_{-0.15}$	$14.77^{+0.30}_{-0.24}$	$19.67^{+0.26}_{-0.22}$
14	$16.68^{+0.12}_{-0.11}$	$17.70^{+0.12}_{-0.12}$	$16.18^{+0.11}_{-0.12}$	$18.31^{+0.16}_{-0.15}$
15	$16.04^{+0.11}_{-0.12}$	$18.51^{+0.18}_{-0.13}$	$15.64^{+0.13}_{-0.13}$	$19.23^{+0.25}_{-0.24}$
16	$15.90^{+0.12}_{-0.11}$	$18.46^{+0.13}_{-0.10}$	$16.25^{+0.12}_{-0.12}$	$18.15^{+0.11}_{-0.12}$
17	$15.81^{+0.11}_{-0.10}$	$17.94^{+0.12}_{-0.12}$	$15.76^{+0.11}_{-0.10}$	$18.00^{+0.12}_{-0.12}$
18	$15.21^{+0.13}_{-0.13}$	$19.22^{+0.13}_{-0.20}$	$14.83^{+0.13}_{-0.13}$	$19.60^{+0.12}_{-0.13}$
19	$14.85^{+0.14}_{-0.13}$	$19.49^{+0.15}_{-0.20}$	$11.33^{+0.13}_{-0.14}$	$19.12^{+0.22}_{-0.27}$
20	$14.67^{+0.14}_{-0.14}$	$19.46^{+0.10}_{-0.10}$	$14.82^{+0.14}_{-0.14}$	$19.35^{+0.10}_{-0.10}$
21	$13.65^{+0.11}_{-0.11}$	$21.54^{+0.26}_{-0.28}$	$13.68^{+0.12}_{-0.12}$	$21.23^{+0.32}_{-0.29}$
22	$14.88^{+0.28}_{-0.23}$	$19.56^{+0.31}_{-0.29}$	$14.30^{+0.14}_{-0.12}$	$20.30^{+0.19}_{-0.23}$
23	$8.84^{+0.12}_{-0.12}$			
24	$15.30^{+0.23}_{-0.43}$	$19.86^{+0.19}_{-0.28}$	$14.12^{+0.12}_{-0.12}$	$20.62^{+0.12}_{-0.11}$
25	$14.64^{+0.15}_{-0.13}$	$19.61^{+0.06}_{-0.06}$	$14.49^{+0.13}_{-0.12}$	$19.68^{+0.06}_{-0.06}$
26	$14.42^{+0.22}_{-0.19}$	$19.58^{+0.11}_{-0.08}$	$14.09^{+0.16}_{-0.13}$	$19.79^{+0.11}_{-0.11}$
27	$13.84^{+0.11}_{-0.12}$	$20.75^{+0.22}_{-0.21}$	$13.32^{+0.12}_{-0.12}$	$21.69^{+0.21}_{-0.21}$
28	$11.02^{+0.14}_{-0.14}$		$13.24^{+0.10}_{-0.10}$	$22.56^{+0.28}_{-0.28}$
29	$7.80^{+0.14}_{-0.14}$		$4.82^{+0.15}_{-0.17}$	
30	$6.12^{+0.21}_{-0.21}$		$3.67^{+0.19}_{-0.19}$	
31	$5.81^{+0.19}_{-0.17}$		$3.67^{+0.17}_{-0.15}$	
32	$9.11^{+0.13}_{-0.13}$		$4.38^{+0.18}_{-0.19}$	

https://doi.org/10.5194/acp-2022-772
Preprint. Discussion started: 17 November 2022

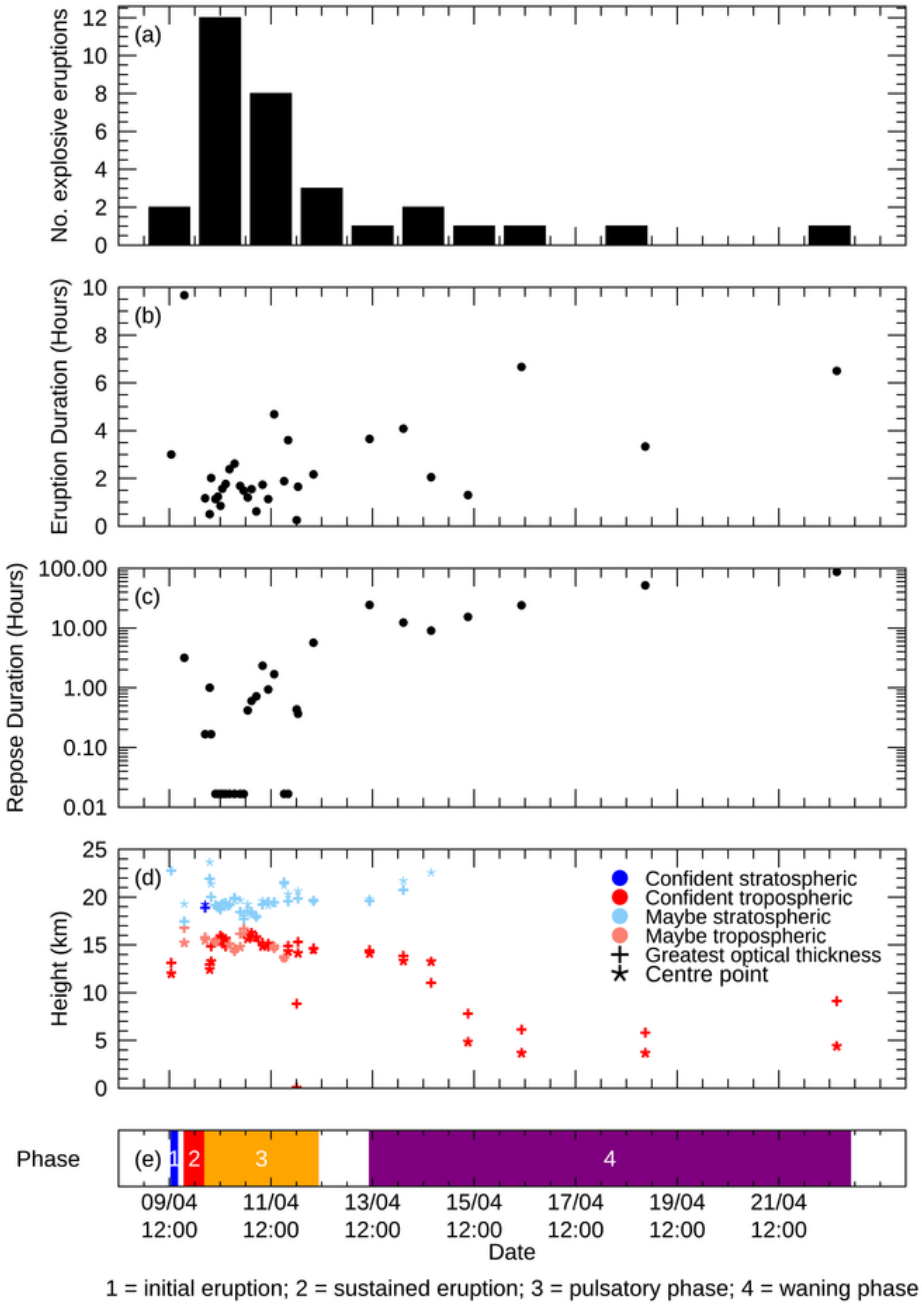

Figure 6. Summary of ABI results. (a) Number of explosive eruptions on each day. (b) Duration of each explosive event. (c) Repose duration between events. (d) Heights retrieved with optically thick and centre BT methods. The colour is used to indicate confidence in tropospheric and stratospheric solutions. (e) Using the ABI data the 2021 eruption has been divided into the four phases with the timing shown here.

https://doi.org/10.5194/acp-2022-772
Preprint. Discussion started: 17 November 2022


Atmospheric Chemistry and Physics Discussions

The eruptive events identified from the ABI data have been split into four phases each with distinct characteristics. The first emission (and first phase of the eruption), is likely to correspond to arrival of gas-rich magma at the surface, and loss of the lava-dome cap. This is seen with ABI at around 12:54 UTC (08:54 LT) on 9 April. This corresponds well with the 08:41 (LT, 12:41 UTC) eruption start time stated in Joseph et al. (2022). Using the ABI data, this emission appears to be relatively short lived lasting around 3 hours, finishing at around 15:54 UTC, and during this time two plumes are evident. The main plume travels to the east-north-east, with a height of around $13.11^{+0.12}_{-0.12}$ km based on the optically thick BT method. This is greater than the 8 km reported by the Belmont Observatory (Global Volcanism Program, 2021b). However, differences between ground based and satellite measurements can arise for a number of reasons including the different viewing angles. During this eruptive episode, a second lower altitude plume can also be seen travelling to the west.

Following a short pause of around 3 hours and 10 minutes, the second phase of the eruption started at around 19:04 UTC on 9 April. This is characterised by a sustained ash emission event with a duration of around 9 hours and 40 minutes. Height estimates based on the BT method are between 15.21 and 19.28 km. In this case the plume direction and the wind profile does not help determine whether the tropospheric or stratospheric solution is more likely. The structures of the plume suggest that there may have been some strong pulses within this sustained phase (see Table 2) but these cannot be resolved from the 10-minute ABI images. The observations using the ABI instrument are generally consistent with those made by Joseph et al. (2022) who mention a "sustained" and "pulsing" explosive phase starting at 16:00 UTC on the 9 April and finishing at 6:00 UTC on 10 April.

The explosive events identified with the ABI instrument suggest that the eruption entered a third phase at 4:54 UTC on 10 April. This phase appears more pulsatory with a further 23 discrete ash emission events identified within a 54 hour period. Joseph et al. (2022) characterise this phase as one of "ash venting". The length of these explosive events identified from the ABI data varied from around 15-minutes to 4 hours and 41 minutes. This style of repetitive ash bursts is similar to the "Vulcanian" explosions documented at multiple andesite volcanoes, which is considered to reflect the rapid sealing, pressurisation and failure of magma within the conduit (e.g. Druitt et al., 2002; Watt et al., 2007; Joseph et al., 2022). The first pulse is shown to most likely be in the stratosphere with height solutions of $18.89^{+0.14}_{-0.19}$ and $19.20^{+0.16}_{-0.14}$ km for the optically thick and centre BT methods respectively. The majority of the remaining pulses in this phase have been labelled as most likely tropospheric or uncertain. Details are shown in Table 3.

The fourth and final phase of the eruption, defined with the ABI data, began on 13 April at 10:36 UTC and continued to the 22 April. During this phase there were a further seven events each lasting a few hours and emitting ash into the troposphere (heights between $3.67^{+0.19}_{-0.19}$ and $14.42^{+0.22}_{-0.19}$ km). Fig. 6d shows that during this phase, the heights for each eruptive event fall suggesting a decrease in eruptive power. The exception is the final event which took place on 22 April where the height obtained is slightly higher than the previous few events. The final eruptive event emitted ash into the lower troposphere for around 6.5 hours. Compared to the earlier phases, the RGB images suggest that the plumes in this waning stage are more optically thin. A number of these explosive events appear to have an explosive eruption which produces a small optically thick cloud, followed by a longer emission of a less optically thick ash cloud.

https://doi.org/10.5194/acp-2022-772
Preprint. Discussion started: 17 November 2022


Atmospheric Chemistry and Physics Discussions

3.2 SO_2 dispersion

The linear and iterative SO_2 retrievals have been applied to IASI spectra from 9 to 30 April 2021. The iterative retrieval column amounts for 9 to 26 April are displayed in Fig. 7. The $\log_{10}$ values are shown to highlight the plume structures. Figure 8 shows examples of the column amount and height outputs from the iterative retrieval for 10 and 11 April. Animations of the iterative retrieval column amount and height outputs for the full time period explored can be found in the supplementary material along with animations showing the error outputs. The mapped results have been obtained by gridding the outputs for all three IASI instruments to a regular 0.125 by 0.125 degree grid. The results have been split into descending (∼9:30 am local overpass time at the equator) and ascending (∼9:30 pm local overpass time at the equator).

Figure 7 shows the $\log_{10}$ of the SO_2 column amounts from the iterative retrieval. In these maps it is possible to see the evolution of the La Soufrière SO_2 plumes between 9 and 26 April. The plume is first apparent as a faintly elevated emission to the east of the volcano in the ascending overpass on 9 April 2021. A stronger signal is then visible in the descending orbits on 10 April fanning out to the east of the volcano across the North Atlantic. By the ascending orbits on 11 April, the plume has travelled across the Atlantic and has almost reached the west coast of Africa. The higher values for the column amounts leading back to the source reflect the frequent eruptive events that occurred over this time period. On the 12 April, while the bulk of the plume is advancing towards the east, a fraction of the plume travels to the south and west of the volcano. Over the next few days the plume continues to be transported both to the east and west of the volcano and by the 21st April the plume has been transported around the circumference of the globe. Figure 9b shows the distribution of the SO_2 mass with latitude. The largest concentration of SO_2 (up to 17 April) is between 0 and 20° N but parts of the plume have reached 45° north and south. This highlights the ability of tropical eruptions to transport SO_2 across both hemispheres, rather than being confined to a narrower latitude band like plumes from eruptions at high latitudes (Schmidt and Black, 2022). Also highlighted in Fig. 9, is a line of elevated SO_2 around 15° S. This is the latitude of Sabancaya volcano (71.857°W, 15.787° S, summit elevation of 5.96 km) in Peru which was erupting throughout the studied time period. Plumes from Sabancaya can be distinguished in the iterative retrieval maps in the supplementary material.

https://doi.org/10.5194/acp-2022-772
Preprint. Discussion started: 17 November 2022

Atmospheric Chemistry and Physics Discussions

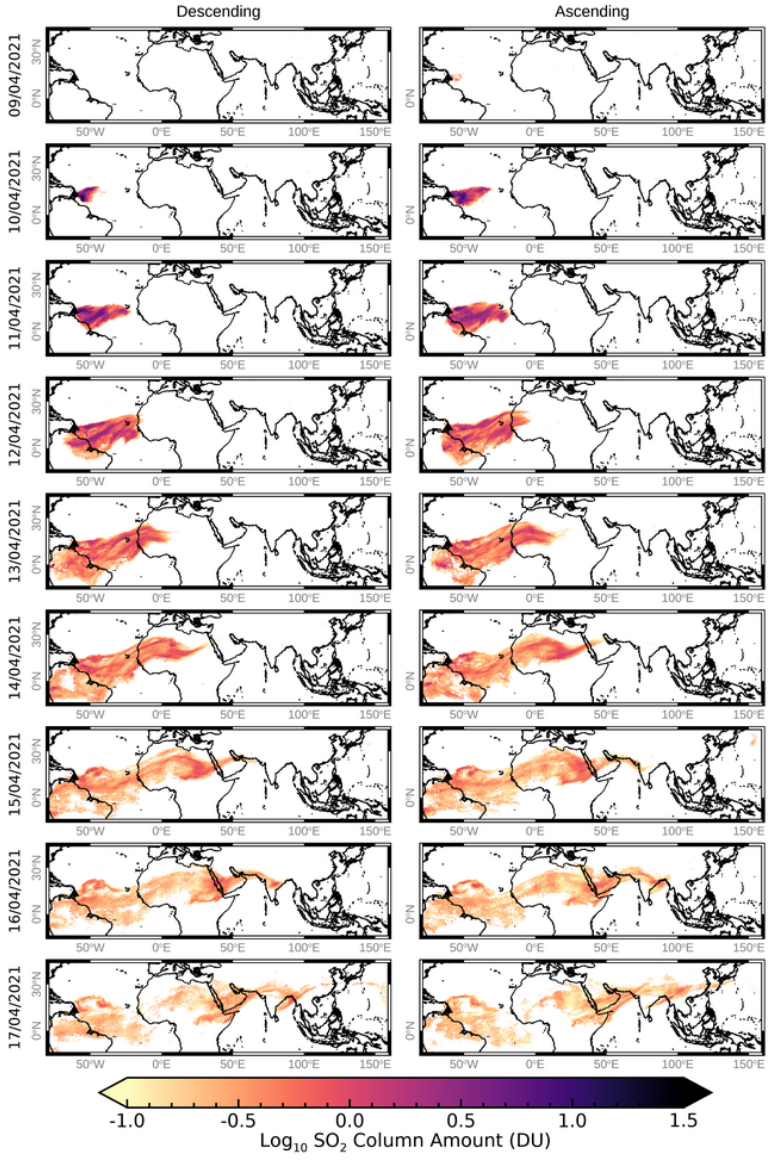

Figure 7. Maps showing the gridded $\log_{10}$ IASI iterative SO_2 retrieval column amount output for 9 to 26 April 2021. Maps on the left show results from the descending orbits (9:30 am local overpass time), while plots on the right show results for the ascending (9:30 pm local overpass time). Note that from 18 April, the geographic region displayed has been expanded to show the full extent of the plumes on these days. The location of the volcano is marked by a black triangle.

https://doi.org/10.5194/acp-2022-772
Preprint. Discussion started: 17 November 2022

Atmospheric Chemistry and Physics Discussions

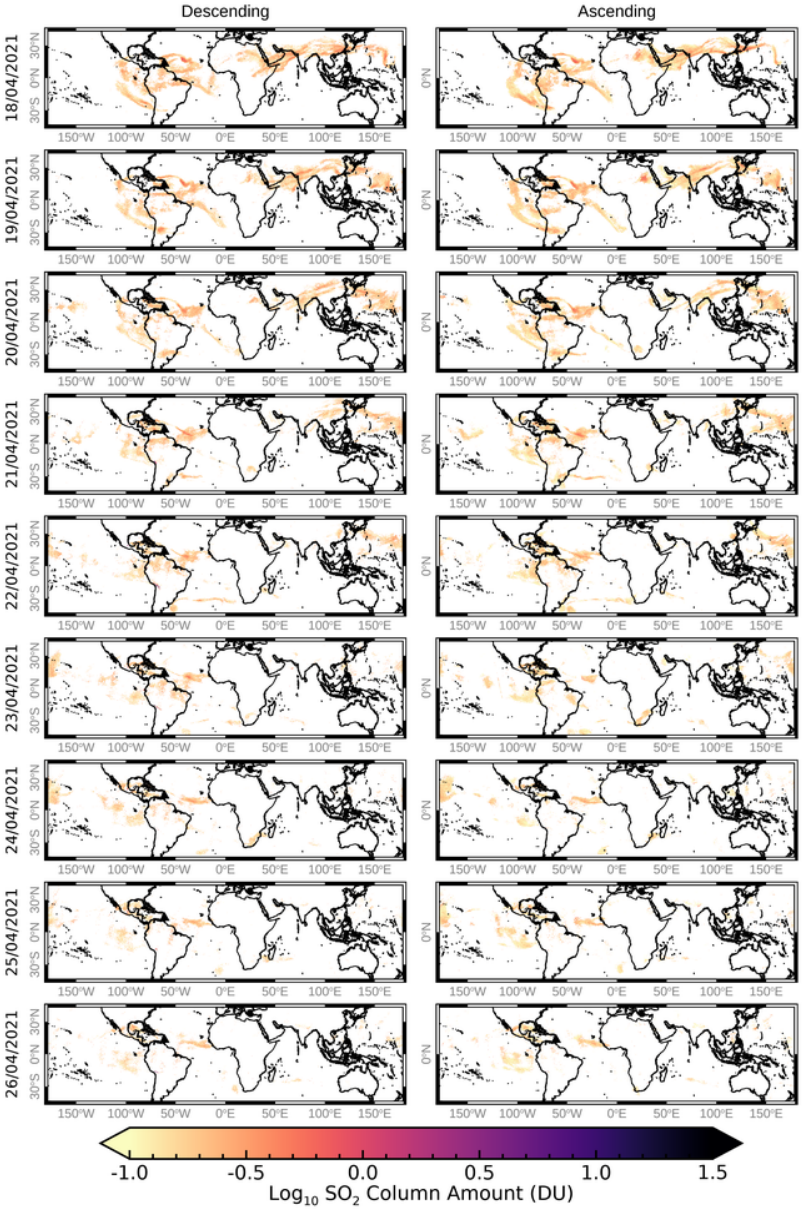

Figure 7. *Continued.*

https://doi.org/10.5194/acp-2022-772
Preprint. Discussion started: 17 November 2022

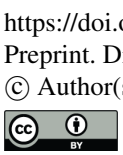

Atmospheric Chemistry and Physics Discussions

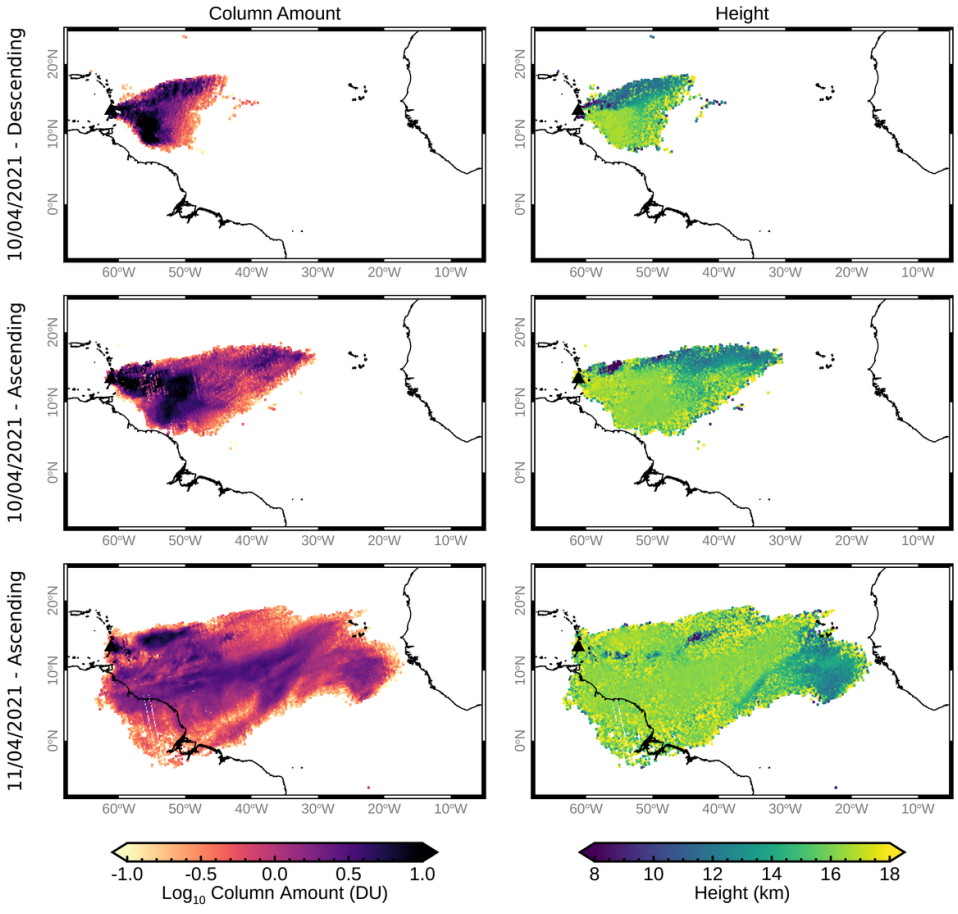

Figure 8. Examples of the IASI SO_2 iterative retrieval gridded column amounts and heights for scenes from the 10 and 11 April 2021. Note that the $\log_{10}$ of the columns amounts are shown to highlight the plume structures. The date and orbit direction are indicated on the left-hand side of the figure. Maps of the results for the entire time period studied can be found in the supplementary information.

https://doi.org/10.5194/acp-2022-772
Preprint. Discussion started: 17 November 2022

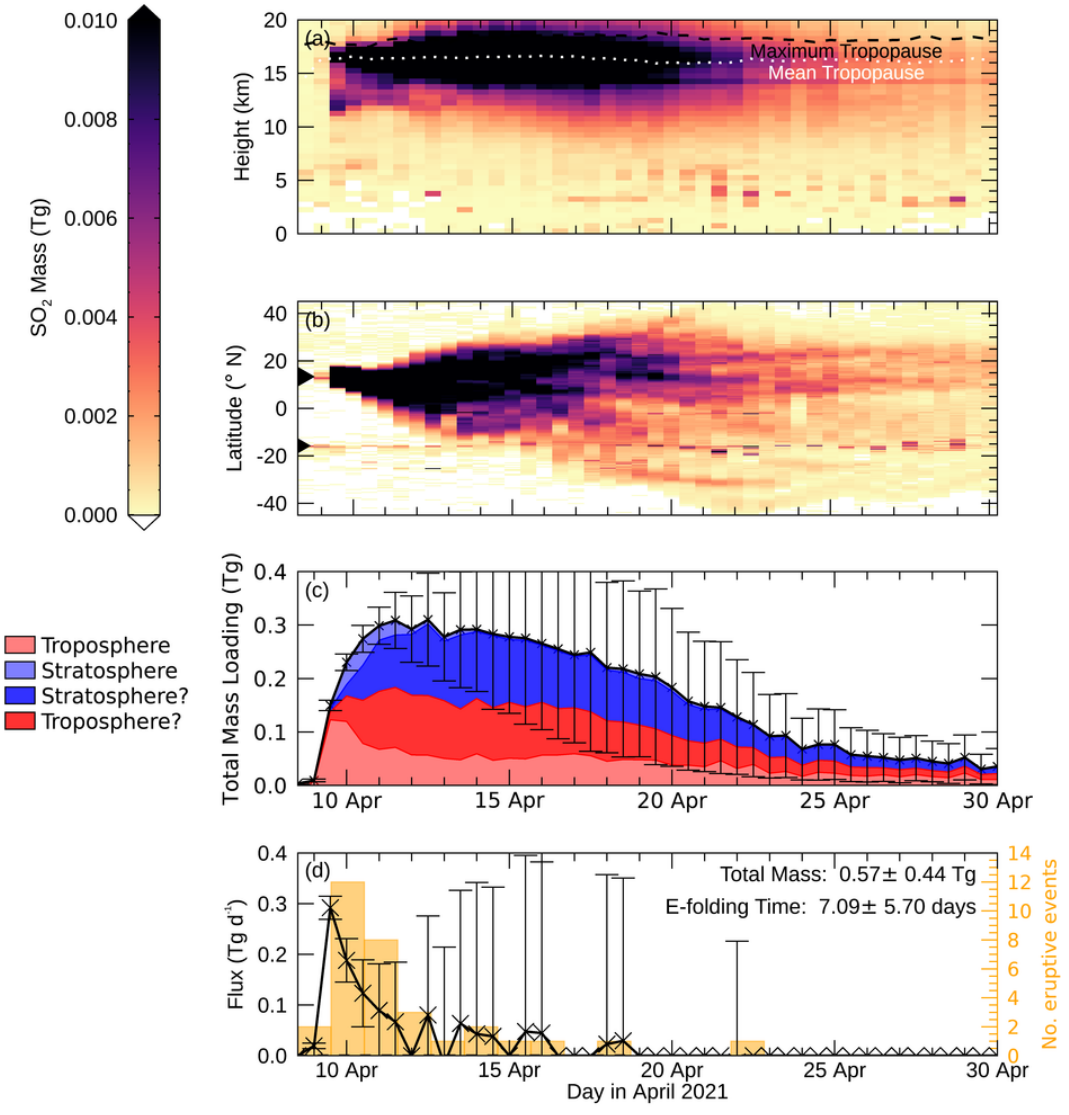

Figure 9. Summary of the IASI SO_2 results generated from iterative retrieval outputs for 9 to 30 April 2021. Each of these has been computed for the -45 to 45° N and -180 and 180° E region. (a) Vertical distribution of the SO_2 mass across the plume with time. The dashed lines show the maximum and mean tropopause heights computed from the ECMWF temperature profiles; (b) Distribution of the SO_2 mass with latitude. The black triangle at 13.33° N indicates the latitude of La Soufrière. The smaller triangle at 15.79° S shows the latitude of Sabancaya in Peru which also erupted during the studied time period; (c) Timeseries of the total mass of SO_2 with errors. Using the retrieved SO_2 heights and the tropopause heights this has been divided into tropospheric and stratospheric SO_2. The height errors have also been used to create two more categories: heights which are stratospheric but given the error could be tropospheric, and heights which are tropospheric but could be stratospheric. (d) The flux of SO_2 with time and the number of eruptive events identified from the ABI data on each day.

https://doi.org/10.5194/acp-2022-772
Preprint. Discussion started: 17 November 2022


Atmospheric Chemistry and Physics Discussions

3.3 SO_2 mass and flux

The total mass of SO_2 over time derived from the IASI iterative retrieval output is shown in Fig. 9c. The mass is computed for following region: -45 to 45° N and -180 and 180° E region. Note that other volcanoes (e.g. Sabancaya in Peru) which were erupting at the same time and whose plumes entered this box are also included in the total mass estimate. However, given these are small plumes their impact is negligible and within the reported errors. The IASI derived SO_2 mass loading peaks at 0.31± 0.09 Tg in the descending orbits on 13 April. The maximum SO_2 mass loading obtained with this IASI SO_2 retrieval for La Soufrière is fairly small compared to other eruptions studied by IASI including Nabro (1.6 Tg), Kasatochi (0.9 Tg), Grímsvötn (0.75 Tg), Copahue (0.72 Tg) and Sarychev (0.6 Tg) in 2011, 2008, 2012 and 2009 respectively (Carboni et al., 2016). It is more similar to the maximum mass loading recorded from Alu Dalafila (0.2 Tg) in November 2008 (Carboni et al., 2016). The fact that the total SO_2 mass loading for La Soufrière peaks a few days after the 2021 eruption began could be linked to the multiple explosive events which occurred between 9 and 13 April leading to an increase in the total atmospheric SO_2 loading: SO_2 emitted at a rate greater than the existing SO_2 declines. The Global Volcanism Program (2021c) reported an early satellite estimate of the SO_2 mass of 0.4 Tg on 10 April: larger than the estimate from IASI on the same day (0.23 ± 0.02 Tg, ascending result). Differences between instruments and retrievals are expected due to the varying sensitivities to SO_2, different height assumptions, the differing effects of volcanic ash and aerosols, different spatial resolutions and observation times. Carn et al. (2016) for example notes that there are often differences between the results from UV and infrared sensors. As mentioned in section 2, the IASI iterative SO_2 retrieval column amounts, and subsequently the total masses, are affected by volcanic ash and instrument sensitivity and so the column amounts and total mass values presented here should be considered minimum estimates.

The SO_2 masses from IASI were converted to flux estimates following the method described in section 2.1.3. The daily SO_2 fluxes computed from the IASI results are shown in Fig. 9d along with the number of explosive events which started on each day as determined with ABI data. Both are also reported in Table 4. There is generally a good correspondence between the number of eruptive events and the SO_2 flux. The greatest flux (0.29 ± 0.02 Tg d^{-1}) from the IASI data occurs on the 10 April in the descending overpasses which incorporates the second eruptive event which had the longest duration. Following this the SO_2 flux derived from IASI data is shown to decrease over the third eruptive phase which ends early on the 12 April. These fluxes agree reasonably well with the flux range reported in Joseph et al. (2022) which varied between 2.76 x 10^5 t d^{-1} (0.276 Tg d^{-1}) on 10 April to 331 t d^{-1} (0.0003 Tg d^{-1}) on 22 April.

By summing the retrieved IASI SO_2 fluxes and multiplying by the time step between the images it is estimated that in total this eruption emitted 0.57±0.47 Tg of SO_2. An alternative way of computing the minimum and maximum total emitted SO_2 is to follow this procedure but add/subtract the flux and error for each time step, rather than sum the errors in quadrature. This gives a minimum and maximum estimates of the total SO_2 mass are 1.94 Tg and 0.24 Tg respectively.

https://doi.org/10.5194/acp-2022-772
Preprint. Discussion started: 17 November 2022

Atmospheric Chemistry and Physics Discussions

Table 4. Number of eruptive events identified with ABI and IASI SO_2 fluxes for 9 to 22 April 2021

		IASI SO_2 flux (Tg d^{-1})	
Date (dd/mm/yyyy)	**Number of eruptive events**	**Descending**	**Ascending**
09/04/2021	2	0.00± 0.00	0.02± 0.01
10/04/2021	12	0.29± 0.02	0.19± 0.04
11/04/2021	8	0.12± 0.07	0.09± 0.09
12/04/2021	3	0.07± 0.12	0.00± 0.00
13/04/2021	1	0.08± 0.20	-0.02± 0.23
14/04/2021	2	0.06± 0.26	0.04± 0.30
15/04/2021	1	0.04± 0.29	0.00± 0.00
16/04/2021	1	0.05± 0.35	0.04± 0.34
17/04/2021	0	0.00± 0.00	0.00± 0.00
18/04/2021	1	0.00± 0.00	0.02± 0.33
19/04/2021	0	0.03± 0.32	0.00± 0.00
20/04/2021	0	0.00± 0.00	0.00± 0.00
21/04/2021	0	0.00± 0.00	0.00± 0.00
22/04/2021	1	0.00± 0.00	-0.01± 0.24

3.4 SO_2 plume heights

Examples of the iterative retrieval height results are shown in Fig. 8. The heights in the descending orbits on 10 April are variable. The heights in the northern edge of the plume (mostly 10 to 13 km, some less than 10 km) are lower than the rest of the plume. The southern part of the SO_2 plume is higher: primarily between 13 and 18 km, and in some cases exceeding this. The results presented here are similar to observations made by the Multi-angle Imaging Spectroradiometer (MISR) on-board the Terra satellite (Yue et al., 2022). Results from this instrument on 10 April showed that there are multiple layers of ash, with two primary layers at 12 and 18 km, and some parts of the plume reaching 20 km (Yue et al., 2022). The IASI results show that the structures within the plume evolve as the plume stretches across the Atlantic with the higher values (15 to 17 km) making up the majority of the image. Note that over time there appears to be more speckle in the height results (see animation in the supplementary files): this reflects increased uncertainty. The variations in height across the entire SO_2 plume are likely to be linked to the multiple injection heights and pulses which occurred during the earlier eruptive events, as discussed in section 3.1. The IASI SO_2 heights are also generally consistent with ash height estimates reported in Global Volcanism Program (2021b) bulletin report; although it should be noted that SO_2 and ash are not always colocated spatially, temporally or in height (e.g. Holasek et al., 1996; Thomas and Prata, 2011; Moxnes et al., 2014; Prata et al., 2017). The lower heights obtained from the ABI data and mentioned in the Global Volcanism Program (2021b) bulletin report, for the later stages of the eruption (e.g. 14-22

https://doi.org/10.5194/acp-2022-772
Preprint. Discussion started: 17 November 2022


Atmospheric Chemistry and Physics Discussions

April), are not reflected in the IASI results. This is potentially because the retrieval has been setup in a way that is optimised for higher plumes, the fact that these eruptive events emitted less SO_2 (below the detection limit of the retrieval), or due to multiple layers of SO_2.

The evolution of the vertical distribution of the SO_2 mass across the plume is shown in Fig. 9a. This is computed from the gridded column amounts (converted to mass values) and the gridded heights for each day (descending and ascending). On 10 April, SO_2 is shown to be emitted at multiple heights: a smaller emission between 11 and 13 km and a larger quantity between 15 and 18 km. The lower layer largely disappears within three days. Between 12 and 18 April the SO_2 mass is shown to be spread over 13 to 19 km. Lines showing the maximum ($\sim$18 km) and average ($\sim$16 km) tropopause heights are displayed in Fig. 9a. This was estimated based on the World Meteorological Organisation's (WMO) definition of the tropopause: that the tropopause occurs at the lowest level where the temperature lapse rate falls beneath 2 K km^{-1} for at least 2 km. Note that this is computed from the tropopause heights for the pixels containing SO_2 and where the iterative retrieval output passes the quality control outlined in section 2.1.2: this means that the number of pixels used in this calculation varies over time. There is more variation in the tropopause heights than would usually be expected which may call for a different metric to be applied in the future to get a more consistent tropopause height from this dataset. For example, based on the sharp changes in wind speed and direction in figure 4, the tropopause would be placed at 17 to 18 km. Much of the SO_2 appears to be in the upper troposphere and around the height of the tropopause which supports the observation made by Carboni et al. (2016) that SO_2 from explosive eruptions often ends up at the tropopause. This observation is consistent with the direction of travel of the plume (to the east) and the wind direction at these heights (which has an easterly direction in the upper troposphere and around the tropopause, Fig. 4a). A fairly persistent lower layer of SO_2 can be observed between 3 and 7 km. Some of this can be attributed to emissions at Sabancaya volcano in Peru. From 19 April a layer can also be observed at 14 to 14.5 km. This is around the height of the *a priori* and so is most likely due to a loss of height information in the IASI spectra as the plume thins.

Figure 9c shows the fraction of SO_2 which has been categorised as either tropospheric or stratospheric. Note that this has been calculated on a pixel by pixel basis using the height of the tropopause calculated from the WMO definition. Also shown in this plot, is the degree of uncertainty with regard to the height of SO_2 relative to the tropopause. Figure 9c highlights that a fraction of the SO_2 mass which while classified as stratospheric could in fact be tropospheric when the errors on the height are considered. Similarly it shows that the fraction of the mass classified as tropospheric which could be stratospheric. In general it appears that there is a similar amount of SO_2 entering the troposphere and stratosphere. For example, in the descending orbits on 13 April, 54.26 % and 45.74 % of the SO_2 was shown to be in the troposphere and stratosphere respectively. However, based on the error bars, 66.34 % of the tropospheric result could also be classed as stratospheric given the overlap of the error bars with the tropopause height, and 94.38 % of the SO_2 classed as stratospheric could be tropospheric. Given lower tropopause heights (based on the ECMWF temperature profiles and WMO definition), it is more likely that the majority of the plume is in the upper troposphere and around the height of the tropopause, with some pushing into the stratosphere. This conclusion is also supported by the vertical distribution shown in Fig. 9a.

The e-folding time of SO_2 varies with a number of factors including the latitude of the volcano, the injection height of the plume, meteorological conditions, cloud cover and season (Schmidt and Black, 2022). Typically, the e-folding time varies from

https://doi.org/10.5194/acp-2022-772
Preprint. Discussion started: 17 November 2022


Atmospheric Chemistry and Physics Discussions

hours to days in the lower troposphere to weeks in the stratosphere. A first estimate of 6.61 days for the e-folding time was estimated by fitting Eq. 1 to the IASI total SO_2 masses between 23 to 28 April 2021. Following the application of the Carboni et al. (2019) method to compute the flux and average e-folding time, the average e-folding time was adjusted to 7.09±5.70 days. This is in line with other eruptions including Jebel at Tair (2007) and Merapi (2010), both volcanoes in the tropics and which emitted plumes between 15 and 18 km, and had e-folding times of between 2 and 4 days (Carn et al., 2016).

4 Comparison with the 1979 eruption

There are a number of similarities between the 1979 and 2021 eruptions at La Soufrière. Shepherd et al. (1979) give a detailed account of the eruptive sequence for the 1979 eruption and report a series of explosive eruptions between 13 and 26 April 1979, with the first explosions occurring from within a water-filled summit crater lake. In the first few hours after the eruption began on the 13 April 1979 (9:30 to 15:00 UTC), continuous emissions of steam were punctuated with explosive eruptions producing ash clouds that reached greater than 8 km (Shepherd et al., 1979). This activity was followed by a series of six explosive events with varying durations between 20:05 on 13 April and 15:50 on 14 April. Estimates from satellite data on 13 and 14 April give ash heights of 17 to 18 km for two of these plumes (Shepherd et al., 1979). Following this, between 14 and 17 April, the volcano entered a new phase with only occasional ash emissions rising 1 to 2 km above the vent. Another explosive event occurred on the 17 April with ash emissions reaching 18.7 km. Following this, the intensity of activity generally declined, although two more explosive events occurred on the 22 and 26 April (Shepherd et al., 1979). By the end of the 1979 explosive sequence, the crater had been infilled with pyroclastic debris, and the summit lake had disappeared. The 2021 explosive eruption sequence shares a number of similarities with the 1979 eruption, even though the early stages of the 2021 eruption were rather different: with 3 months of dome effusion into a "dry" summit crater. Both the 1979 and 2021 eruptions consisted of a series of explosive events and both had a pulsatory phase in the first few days after the start of the eruption: although notably a larger number of discrete events occurred during the 2021 eruptive period. The later eruptive events in both the 1979 and 2021 eruptions had a longer repose time.

Another similarity between the 1979 and 2021 eruptive periods are the plume heights. Measurements of the 1979 heights were far sparser: with estimates coming from relatively infrequent satellite data, ground/ship based observations and aircraft observations. As mentioned above, Shepherd et al. (1979) gives height estimates for individual eruptive events ranging between 8 and 18.7 km. This is similar to this study which reports a fairly wide range of heights for the 2021 eruption. Krueger (1982) used SMS-1 satellite data to estimate that part of the plume exceeded 18 km: placing it in the stratosphere. Another study using an airborne LiDAR by Fuller et al. (1982) showed layers of ash between 16 and 19.5 km. These heights for ash are in a similar range to those for SO_2 reported in this study, although again the difficulty of using ash as a proxy for SO_2 is noted. While both Krueger (1982) and Fuller et al. (1982) indicate that parts of the plume reached the stratosphere it is possible that there was significant variability across the full extent of the plume which was unmeasured, and so it is difficult to quantify how much of the plume was tropospheric and stratospheric for the 1979 eruption.

https://doi.org/10.5194/acp-2022-772
Preprint. Discussion started: 17 November 2022


Atmospheric Chemistry and Physics Discussions

A significant difference between the two eruptions is the quantity of SO_2 observed by satellite instruments. The 1979 eruption of La Soufrière is one of the first observations of volcanic SO_2 made by the Total Ozone Monitoring Instrument (TOMS) but elevated emissions were only seen on 2 days (Carn et al., 2003). In total only ∼3 kt of SO_2 was measured with TOMS (Carn et al., 2016): substantially lower than the estimates reported here from IASI for the 2021 eruption. Carn et al. (2016) indicates that the TOMS SO_2 estimate is only a fraction of the total emitted with Scaillet et al. (2003) obtaining a total sulfur mass of 0.46 Tg based on petrological methods (∼ 1 Tg SO_2; Carn et al. 2016). Carn et al. (2016) suggests that the majority of sulfur emission may have been in the form of H_2S, with slow oxidation preventing SO_2 detection with TOMS. It is also possible that part of the low SO_2 mass estimate from TOMS could be attributed to the lower resolution of the instrument compared to the satellite instruments observing the 2021 eruption.

5 Conclusions

The April 2021 eruption of La Soufrière emitted large plumes of ash and SO_2 into the atmosphere. Satellite data offers unique insights into these emissions. Using data from ABI it is possible to identify the emission of ash, and in this study the instrument's high temporal resolution (up to 1-minute) was used to identify and characterise different phases of the April 2021 La Soufrière eruption. Careful examination of true and false colour images, and BTD maps, allowed the identification of the start and end times of 32 explosive events that took place during eruption: although this should be considered a minimum estimate. Based on these observations four eruptive phases have been identified: (1) An initial explosive event producing a ash cloud; (2) a strong and sustained ash emission lasting several hours and producing a large optically thick ash cloud; (3) a pulsatory phase with 23 discrete explosive events in a 54 hour period, varying in duration between 15 minutes and 4 hours, each producing optically thick ash clouds; (4) a waning phase with 7 eruptive events with lower plume heights, optically thinner ash clouds and greater durations between explosive events.

Measurements with retrievals developed for the IASI satellite instrument were able to track the plumes of SO_2 from the 2021 La Soufrière eruption for several weeks after the first eruption occurred. A peak value of 0.31±0.09 Tg was obtained for the total SO_2 mass burden on 13 April. However, it is likely that this is an underestimate due to the effects of volcanic ash on the results and the presence of SO_2 below the detection limit of the instrument. Using the daily IASI SO_2 fluxes it was possible to estimate the total emission of SO_2 to the atmosphere which was 0.57±0.44 Tg with an upper and lower limit of 1.94 and 0.24 Tg respectively (considering the full extent of the uncertainties on each day). Again these should be considered minimum estimates. The retrieved heights show interesting structures in the plume that reflect the multiple eruptive pulses and different injection heights: consistent with observations on the ground and made by other satellite instruments. The majority of the SO_2 was emitted between 13 and 19 km. The height results suggest that the majority of SO_2 was emitted into the upper troposphere and lower stratosphere.

The 2021 eruption showed some remarkable similarities with the 1979 eruption both in terms of the height and the eruptive sequence. This emphasises the importance of studying these eruptions, utilising as many data sources as possible, in order to

https://doi.org/10.5194/acp-2022-772
Preprint. Discussion started: 17 November 2022


Atmospheric Chemistry and Physics Discussions

better understand the volcano and the character of its eruptions so as to be better prepared for future eruptive events (e.g. Joseph et al., 2022; Barclay et al., 2022).

Data availability. GOES-16 satellite data are available through NOAA's Big Data Program (https://www.noaa.gov/information-technology/open-data-dissemination; webpage last access on 9 November 2022). The IASI level 1c data are available from EUMETSAT. The meteorological profiles used in this study are from ECMWF. The authors plan to archive the IASI SO_2 results following completion of the peer review process. In the meantime they can be found at http://eodg.atm.ox.ac.uk/IASI/la_soufriere/ (webpage last access on 8 November 2022). The map animations for each eruptive event created with the ABI data will also be archived following the review process but in the meantime can be accessed at http://eodg.atm.ox.ac.uk/ABI/la_soufriere/ (webpage last accessed on 8 November 2022).

Author contributions. The IASI SO_2 retrievals and ash linear retrieval were run by IAT with guidance from RGG. The ABI images were studied by both IAT and SRP. ATP and SRP provided guidance on using the ABI data. IAT obtained height information from the ABI data, did the flux analysis and produced the figures. TAM and DMP provided insights into the volcanological processes and historical context of this eruption. All authors contributed to discussion of results and editing of the manuscript.

Competing interests. There are no competing interests

Acknowledgements. We are grateful to EUMETSAT for the provision of the IASI data, and to ECMWF for the meteorological data used. These datasets were accessed at the Centre for Environmental Data Analysis (CEDA) (EUMETSAT , 2009, 2014, 2021; European Centre for Medium-Range Weather Forecasts, 2012, 2021). The JASMIN data analysis facility was used to run the IASI retrievals and to run the code estimating the heights from ABI. We also acknowledge the NOAA big data programme for making the GOES ABI data available.
I.A.T., R.G.G., T.A.M. and D.M.P. acknowledge the support of the NERC Centre for the Observation and Modelling of Earthquakes, Volcanoes and Tectonics (COMET), a partnership between UK Universities and the British Geological Survey. This study was in part funded through NERC's support of the National Centre for Earth Observation (NCEO). I.A.T., R.G.G. and T.A.M. were supported by the Natural Environment Research Council (NERC) project VPLUS (NE/S004025/1). A.T.P. and R.G.G. were supported by the NERC project R4-Ash (NE/S003843/1). S.R.P.'s work on this study was funded as part of NERC's support of the National Centre for Earth Observation, award ref. NE/R016518/1; and by a NERC Innovation fellowship, award ref. NE/R013144/1. D.M.P. acknowledges support from NERC Urgency grant NE/W000725/1. D.M.P. thanks Dan Goss, Jenni Barclay and Pat Joseph for discussions. I.A.T. thanks Anu Dudhia, Elisa Carboni and Richard Siddans for some of the code used.

https://doi.org/10.5194/acp-2022-772
Preprint. Discussion started: 17 November 2022

Atmospheric Chemistry and Physics Discussions

References

Ackerman, S. A., Schreiner, A. J., Schmit, T. J., Woolf, H. M., Li, J., and Pavolonis, M.: Using the GOES Sounder to monitor upper level SO_2 from volcanic eruptions, Journal of Geophysical Research: Atmospheres, 113, https://doi.org/10.1029/2007JD009622, 2008.

Aspinall, W., Sighurdsson, H., and Shepherd, J.: Eruption of Soufrière Volcano on St. Vincent Island, 1971-1972, Science, 181, 117–124, https://doi.org/10.1126/science.181.4095.117, 1973.

Aubry, T. J., Engwell, S., Bonadonna, C., Carazzo, G., Scollo, S., Van Eaton, A. R., Taylor, I. A., Jessop, D., Eychenne, J., Gouhier, M., Mastin, L. G., Wallace, K. L., Biass, S., Bursik, M., Grainger, R. G., Jellinek, A. M., and Schmidt, A.: The Independent Volcanic Eruption Source Parameter Archive (IVESPA, version 1.0): A new observational database to support explosive eruptive column model validation and development, Journal of Volcanology and Geothermal Research, 417, 107 295, https://doi.org/10.1016/j.jvolgeores.2021.107295, 2021.

Barclay, J., Robertson, R., Scarlett, J. P., Pyle, D. M., and Armijos, M. T.: Disaster aid? Mapping historical responses to volcanic eruptions from 1800–2000 in the English-speaking Eastern Caribbean: their role in creating vulnerabilities, Disasters, 46, S10–S50, https://doi.org/10.1111/disa.12537, 2022.

Blumstein, D., Chalon, G., Carlier, T., Buil, C., Hebert, P., Maciaszek, T., Ponce, G., Phulpin, T., Tournier, B., Simeoni, D., Astruc, P., Clauss, A., Kayal, G., and Jegou, R.: IASI instrument: Technical overview and measured performances, Proceedings of SPIE - The International Society of the Optical Engineering, 5543, 196–207, https://doi.org/10.1117/12.560907, 2004.

Brazier, S., Davis, A., Sigurdsson, H., and Sparks, R.: Fall-out and deposition of volcanic ash during the 1979 explosive eruption of the soufriere of St. Vincent, Journal of Volcanology and Geothermal Research, 14, 335–359, https://doi.org/10.1016/0377-0273(82)90069-5, 1982.

Carboni, E., Grainger, R., Walker, J., Dudhia, A., and Siddans, R.: A new scheme for sulphur dioxide retrieval from IASI measurements: application to the Eyjafjallajökull eruption of April and May 2010, Atmospheric Chemistry and Physics, 12, 11 417–11 434, https://doi.org/10.5194/acp-12-11417-2012, 2012.

Carboni, E., Grainger, R. C., Mather, T. A., Pyle, D. M., Thomas, G., Siddans, R., Smith, A., Dudhia, A., Koukouli, M. L., and Balis, D.: The vertical distribution of volcanic SO_2 plumes measured by IASI, Atmospheric Chemistry and Physics, 16, 4343–4367, https://doi.org/10.5194/acp-16-4343-2016, 2016.

Carboni, E., Mather, T. A., Schmidt, A., Grainger, R. G., Pfeffer, M. A., Ialongo, I., and Theys, N.: Satellite-derived sulfur dioxide (SO_2) emissions from the 2014–2015 Holuhraun eruption (Iceland), Atmospheric Chemistry and Physics, 19, 4851–4862, https://doi.org/10.5194/acp-19-4851-2019, 2019.

Carn, S., Krueger, A., Bluth, G., Schaefer, S., Krotkov, N., Watson, I., and Datta, S.: Volcanic eruption detection by the Total Ozone Mapping Spectrometer (TOMS) instruments: a 22-year record of sulphur dioxide and ash emissions, pp. 177–202, Geological Society, London, https://doi.org/10.1144/GSL.SP.2003.213.01.11, 2003.

Carn, S., Clarisse, L., and Prata, A.: Multi-decadal satellite measurements of global volcanic degassing, Journal of Volcanology and Geothermal Research, 311, 99–134, https://doi.org/10.1016/j.jvolgeores.2016.01.002, 2016.

Clarisse, L., Coheur, P.-F., Prata, A. J., Hurtmans, D., Razavi, A., Phulpin, T., Hadji-Lazaro, J., and Clerbaux, C.: Tracking and quantifying volcanic SO_2 with IASI, the September 2007 eruption at Jebel at Tair, Atmospheric Chemistry and Physics, 8, 7723–7734, https://doi.org/10.5194/acp-8-7723-2008, 2008.

https://doi.org/10.5194/acp-2022-772
Preprint. Discussion started: 17 November 2022

Clarisse, L., Prata, F., Lacour, J.-L., Hurtmans, D., Clerbaux, C., and Coheur, P.-F.: A correlation method for volcanic ash detection using hyperspectral infrared measurements, Geophysical Research Letters, 37, L19 806, https://doi.org/10.1029/2010GL044828, 2010a.

Clarisse, L., Hurtmans, D., Prata, A. J., Karagulian, F., Clerbaux, C., De Mazière, M., and Coheur, P.-F.: Retrieving radius, concentration, optical depth, and mass of different types of aerosols from high-resolution infrared nadir spectra, Applied optics, 49, 3713–3722, https://doi.org/10.1364/AO.49.003713, 2010b.

Clarisse, L., Coheur, P.-F., Chefdeville, S., Lacour, J.-L., Hurtmans, D., and Clerbaux, C.: Infrared satellite observations of hydrogen sulfide in the volcanic plume of the August 2008 Kasatochi eruption, Geophysical Research Letters, 38, https://doi.org/10.1029/2011GL047402, 2011.

Clarisse, L., Hurtmans, D., Clerbaux, C., Hadji-Lazaro, J., Ngadi, Y., and Coheur, P.-F.: Retrieval of sulphur dioxide from the Infrared Atmospheric Sounding Interferometer (IASI), Atmospheric Measurement Techniques, 5, 581–594, https://doi.org/10.5194/amt-5-581-2012, 2012.

Clarisse, L., Coheur, P.-F., Theys, N., Hurtmans, D., and Clerbaux, C.: The 2011 Nabro eruption, a SO_2 plume height analysis using IASI measurements, Atmospheric Chemistry and Physics, 14, 3095–3111, https://doi.org/10.5194/acp-14-3095-2014, 2014.

Clerbaux, C., Boynard, A., Clarisse, L., George, M., Hadji-Lazaro, J., Herbin, H., Hurtmans, D., Pommier, M., Razavi, A., Turquety, S., Wespes, C., and Coheur, P.-F.: Monitoring of atmospheric composition using the thermal infrared IASI/MetOp sounder, Atmospheric Chemistry and Physics, 9, 6041–6054, https://doi.org/10.5194/acp-9-6041-2009, 2009.

Druitt, T. H., Young, S. R., Baptie, B., Bonadonna, C., Calder, E. S., Clarke, A. B., Cole, P. D., Harford, C. L., Herd, R. A., Luckett, R., Ryan, G., and Voight, B.: Episodes of cyclic Vulcanian explosive activity with fountain collapse at Soufrière Hills Volcano, Montserrat, Geological Society, London, Memoirs, 21, 281–306, https://doi.org/10.1144/GSL.MEM.2002.021.01.13, 2002.

EODG: Animations of ABI results for La Soufriere, http://eodg.atm.ox.ac.uk/ABI/la_soufriere/, accessed: 2022-11-08, 2022.

EUMETSAT : IASI atmospheric spectra (L1C product) from the EPS Metop-A satellite: CEDA mirror archive for STFC, NCAS, NCEO. EUMETSAT, https://catalogue.ceda.ac.uk/uuid/ea46600afc4559827f31dbfbb8894c2e, accessed: 2022-06-28, 2009.

EUMETSAT : IASI atmospheric spectra (L1C product) from the EPS Metop-B satellite: CEDA mirror archive for STFC, NCAS, NCEO. NERC Earth Observation Data Centre, https://catalogue.ceda.ac.uk/uuid/0092c4fe29f76c1b99b4dc19133f361a, accessed: 2022-06-28, 2014.

EUMETSAT : IASI atmospheric spectra (L1C product) from the EPS Metop - C satellite: CEDA mirror archive for STFC, NCAS, NCEO. EUMETSAT, https://catalogue.ceda.ac.uk/uuid/58648f7210c84c44a91dc128d8d750d8, accessed: 2022-06-28, 2021.

European Centre for Medium-Range Weather Forecasts: ECMWF Operational Regular Gridded Data at 1.125 degrees resolution. NCAS British Atmospheric Data Centre, https://catalogue.ceda.ac.uk/uuid/a67f1b4d9db7b1528b800ed48198bdac, accessed: 2022-06-28, 2012.

European Centre for Medium-Range Weather Forecasts: ECMWF ERA5: model level analysis parameter data. Centre for Environmental Data Analysis, https://catalogue.ceda.ac.uk/uuid/f809e61a61ee4eb9a64d4957c3e5bfac, accessed: 2022-06-28, 2021.

Fiske, R. and Sigurdsson, H.: Soufriere Volcano, St. Vincent: Observations of Its 1979 Eruption from the Ground, Aircraft, and Satellites, 216, 1105–1106, https://doi.org/10.1126/science.216.4550.1105, 1982.

Fuller, W. H., Sokol, S., and Hunt, W. H.: Airborne Lidar Measurements of the Soufriere Eruption of 17 April 1979, Science, 216, 1113–1115, https://doi.org/10.1126/science.216.4550.1113, 1982.

Global Volcanism Program: Report on Soufrière St. Vincent (Saint Vincent and the Grenadines) — March 2021 (Bennis, K.L., and Venzke, E., eds.), Bulletin of the Global Volcanism Network, 46:3. Smithsonian Institution, https://doi.org/10.5479/si.GVP.BGVN202103-360150, 2021a.

https://doi.org/10.5194/acp-2022-772
Preprint. Discussion started: 17 November 2022

Atmospheric Chemistry and Physics Discussions

Global Volcanism Program: Report on Soufrière St. Vincent (Saint Vincent and the Grenadines) (Bennis, K.L., and Venzke, E., eds.), Bulletin of the Global Volcanism Network, 46:5. Smithsonian Institution, https://doi.org/10.5479/si.GVP.BGVN202105-360150, 2021b.

Global Volcanism Program: Report on Soufriere St. Vincent (Saint Vincent and the Grenadines). In: Sennert, S K (ed.), Weekly Volcanic Activity Report, 7 April-13 April 2021, Bulletin of the Global Volcanism Network, Smithsonian Institution and US Geological Survey, https://volcano.si.edu/showreport.cfm?wvar=GVP.WVAR20210407-360150, 2021c.

Guermazi, H., Sellitto, P., Cuesta, J., Eremenko, M., Lachatre, M., Mailler, S., Carboni, E., Salerno, G., Caltabiano, T., Menut, L., Serbaji, M. M., Rekhiss, F., and Legras, B.: Quantitative Retrieval of Volcanic Sulphate Aerosols from IASI Observations, Remote Sensing, 13, https://doi.org/10.3390/rs13091808, 2021.

Holasek, R. E., Woods, A. W., and Self, S.: Experiments on gas-ash separation processes in volcanic umbrella plumes, Journal of Volcanology and Geothermal Research, 70, 169–181, https://doi.org/10.1016/0377-0273(95)00054-2, 1996.

Horváth, A., Carr, J. L., Wu, D. L., Bruckert, J., Hoshyaripour, G. A., and Buehler, S. A.: Measurement report: Plume heights of the April 2021 La Soufrière eruptions from GOES-17 side views and GOES-16–MODIS stereo views, Atmospheric Chemistry and Physics, 22, 12 311–12 330, https://doi.org/10.5194/acp-22-12311-2022, 2022.

Joseph, E., Camejo-Harry, M., Christopher, T., C.-A. R., Edwards, S., Graham, O., Johnson, M., Juman, A., Latchman, J. L., Lynch, L., Miller, V. L., Papadopoulos, I., Pascal, K., Robertson, R., Ryan, G., Stinton, A., Grandin, R., Hamling, I., Jo, M.-J., Barclay, J., Cole, P., Davies, B., and Sparks, R.: Responding to eruptive transitions during the 2020–2021 eruption of La Soufrière volcano, St. Vincent, Nature Communications, 13, https://doi.org/10.1038/s41467-022-31901-4, 2022.

Krueger, A. F.: Geostationary Satellite Observations of the April 1979 Soufriere Eruptions, Science, 216, 1108–1109, https://doi.org/10.1126/science.216.4550.1108, 1982.

Lechner, P., Tupper, A., Guffanti, M., Loughlin, S., and Casadevall, T.: Volcanic Ash and Aviation—The Challenges of Real-Time, Global Communication of a Natural Hazard, pp. 1–14, Advances in Volcanology, Springer, Berlin, Heidelberg, https://doi.org/10.1007/11157_2016_49, 2017.

Lindsey, D., Schmit, T. J., MacKenzie, W. M., Jewitt, C. P., Gunshor, M. M., and Grasso, L.: 10.35 μm: atmospheric window on the GOES-R Advanced Baseline Imager with less moisture attenuation, Journal of Applied Remote Sensing, 6, 063 598, https://doi.org/10.1117/1.JRS.6.063598, 2012.

Maes, K., Vandenbussche, S., Klüser, L., Kumps, N., and de Mazière, M.: Vertical Profiling of Volcanic Ash from the 2011 Puyehue Cordón Caulle Eruption Using IASI, Remote Sensing, 8, https://doi.org/10.3390/rs8020103, 2016.

Martínez-Alonso, S., Deeter, M. N., Worden, H. M., Clerbaux, C., Mao, D., and Gille, J. C.: First satellite identification of volcanic carbon monoxide, Geophysical Research Letters, 39, https://doi.org/10.1029/2012GL053275, 2012.

McCormick, M. P., Kent, G. S., Yue, G. K., and Cunnold, D. M.: Stratospheric Aerosol Effects from Soufriere Volcano as Measured by the SAGE Satellite System, Science, 216, 1115–1118, https://doi.org/10.1126/science.216.4550.1115, 1982.

Moxnes, E. D., Kristiansen, N. I., Stohl, A., Clarisse, L., Durant, A., Weber, K., and Vogel, A.: Separation of ash and sulfur dioxide during the 2011 Grímsvötn eruption, Journal of Geophysical Research: Atmospheres, 119, 7477–7501, https://doi.org/10.1002/2013JD021129, 2014.

Oppenheimer, C.: Review article: Volcanological applications of meteorological satellites, International Journal of Remote Sensing, 19, 2829–2864, https://doi.org/10.1080/014311698214307, 1998.

https://doi.org/10.5194/acp-2022-772
Preprint. Discussion started: 17 November 2022

Atmospheric Chemistry and Physics Discussions

Pavolonis, M. J., Sieglaff, J. M., and Cintineo, J. L.: Chapter 10 - Remote Sensing of Volcanic Ash with the GOES-R Series, in: The GOES-R Series, edited by Goodman, S. J., Schmit, T. J., Daniels, J., and Redmon, R. J., pp. 103–124, Elsevier, https://doi.org/10.1016/B978-0-12-814327-8.00010-X, 2020.

Prata, A.: Observations of volcanic ash clouds in the 10-12 μm window using AVHRR/2 data, International Journal of Remote Sensing, 10, 751–761, https://doi.org/10.1080/01431168908903916, 1989a.

Prata, A. and Tupper, A.: Aviation hazards from volcanoes: the state of the science, Natural Hazards, 51, 239–244, https://doi.org/10.1007/s11069-009-9415-y, 2009.

Prata, A. J.: Infrared radiative transfer calculations for volcanic ash clouds, Geophysical Research Letters, 16, 1293–1296, https://doi.org/10.1029/GL016i011p01293, 1989b.

Prata, A. J. and Grant, I. F.: Retrieval of microphysical and morphological properties of volcanic ash plumes from satellite data: Application to Mt Ruapehu, New Zealand, Quarterly Journal of the Royal Meteorological Society, 127, 2153–2179, https://doi.org/10.1002/qj.49712757615, 2001.

Prata, A. T., Grainger, R. G., Taylor, I. A., Povey, A. C., Proud, S. R., and Poulsen, C. A.: Uncertainty-bounded estimates of ash cloud properties using the ORAC algorithm: application to the 2019 Raikoke eruption, Atmospheric Measurement Techniques, 15, 5985–6010, https://doi.org/10.5194/amt-15-5985-2022, 2022.

Prata, F., Bluth, G., Rose, B., Schneider, D., and Tupper, A.: Comments on "Failures in detecting volcanic ash from a satellite-based technique", Remote Sensing of Environment, 78, 341–346, https://doi.org/10.1016/S0034-4257(01)00231-0, 2001.

Prata, F., Woodhouse, M., Huppert, H. E., Prata, A., Thordarson, T., and Carn, S.: Atmospheric processes affecting the separation of volcanic ash and SO_2 in volcanic eruptions: inferences from the May 2011 Grímsvötn eruption, Atmospheric Chemistry and Physics, 17, 10 709–10 732, https://doi.org/10.5194/acp-17-10709-2017, 2017.

Pyle, D. M.: What Can We Learn from Records of Past Eruptions to Better Prepare for the Future?, pp. 445–462, Springer, Cham, https://doi.org/10.1007/11157_2017_5, 2017.

Ravindra Babu, S., Nguyen, L. S. P., Sheu, G.-R., Griffith, S. M., Pani, S. K., Huang, H.-Y., and Lin, N.-H.: Long-range transport of La Soufrière volcanic plume to the western North Pacific: Influence on atmospheric mercury and aerosol properties, Atmospheric Environment, 268, 118 806, https://doi.org/10.1016/j.atmosenv.2021.118806, 2022.

Robertson, R.: An assessment of the risk from future eruptions of the Soufriere volcano of St. Vincent, West Indies, Natural Hazards, 11, 163–191, https://doi.org/10.1007/BF00634531, 1995.

Rose, W. I., Delene, D. J., Schneider, D. J., Bluth, G. J. S., Krueger, A. J., Sprod, I., McKee, C., Davies, H. L., and Ernst, G. G. J.: Ice in the 1994 Rabaul eruption cloud: implications for volcano hazard and atmospheric effects, Nature, 375, 477–479, https://doi.org/10.1038/375477a0, 1995.

Scaillet, B., Luhr, J. F., and Carroll, M. R.: Petrological and Volcanological Constraints on Volcanic Sulfur Emissions to the Atmosphere, pp. 11–40, American Geophysical Union (AGU), https://doi.org/10.1029/139GM02, 2003.

Schmidt, A. and Black, B. A.: Reckoning with the Rocky Relationship Between Eruption Size and Climate Response: Toward a Volcano-Climate Index, Annual Review of Earth and Planetary Sciences, 50, 627–661, https://doi.org/10.1146/annurev-earth-080921-052816, 2022.

Schmit, T. J., Gunshor, M. M., Menzel, W. P., Gurka, J. J., Li, J., and Bachmeier, A. S.: Introducing the Next-Generation Advanced Baseline Imager on GOES-R, Bulletin of the American Meteorological Society, 86, 1079 – 1096, https://doi.org/10.1175/BAMS-86-8-1079, 2005.

https://doi.org/10.5194/acp-2022-772
Preprint. Discussion started: 17 November 2022

Sears, T., Thomas, G., Carboni, E., Smith, A., and Grainger, R.: SO_2 as a possible proxy for volcanic ash in aviation hazard avoidance, Journal of Geophysical Research: Atmospheres, 118, 5698-5709, https://doi.org/10.1002/jgrd.50505, 2013.

Shepherd, J. and Sigurdsson, H.: Mechanism of the 1979 explosive eruption of soufriere volcano, St. Vincent, Journal of Volcanology and Geothermal Research, 13, 119–130, https://doi.org/10.1016/0377-0273(82)90023-3, 1982.

Shepherd, J., Aspinall, W., Rowley, K., Pereira, J., Sigurdsson, H., Fiske, R., and Tomblin, J.: The eruption of Soufrière volcano, St Vincent April–June 1979, Nature, 282, 24–28, https://doi.org/10.1038/282024a0, 1979.

Simpson, J. J., Hufford, G., Pieri, D., and Berg, J.: Failures in Detecting Volcanic Ash from a Satellite-Based Technique, Remote Sensing of Environment, 72, 191–217, https://doi.org/10.1016/S0034-4257(99)00103-0, 2000.

Smart, D. and Sales, T.: Volcanic lightning observed at La Soufrière, Saint Vincent and the Grenadines, Lesser Antilles, Weather, 76, 277–278, https://doi.org/10.1002/wea.4021, 2021.

Taylor, I. A., Carboni, E., Ventress, L. J., Mather, T. A., and Grainger, R. G.: An adaptation of the CO_2 slicing technique for the Infrared Atmospheric Sounding Interferometer to obtain the height of tropospheric volcanic ash clouds, Atmospheric Measurement Techniques, 12, 3853–3883, https://doi.org/10.5194/amt-12-3853-2019, 2019.

Thomas, H. E. and Prata, A. J.: Sulphur dioxide as a volcanic ash proxy during the April–May 2010 eruption of Eyjafjallajökull Volcano, Iceland, Atmospheric Chemistry and Physics, 11, 6871–6880, https://doi.org/10.5194/acp-11-6871-2011, 2011.

Thomas, H. E. and Watson, I. M.: Observations of volcanic emissions from space: current and future perspectives, Natural Hazards, 54, 323–354, https://doi.org/10.1007/s11069-009-9471-3, 2010.

Thompson, J. O., Contreras-Arratia, R., Befus, K. S., and Ramsey, M. S.: Thermal and seismic precursors to the explosive eruption at La Soufrière Volcano, St. Vincent in April 2021, Earth and Planetary Science Letters, 592, 117 621, https://doi.org/10.1016/j.epsl.2022.117621, 2022.

Ventress, L. J., McGarragh, G., Carboni, E., Smith, A. J., and Grainger, R. G.: Retrieval of ash properties from IASI measurements, Atmospheric Measurement Techniques, 9, 5407–5422, https://doi.org/10.5194/amt-9-5407-2016, 2016.

Walker, J., Dudhia, A., and Carboni, E.: An effective method for the detection of trace species demonstrated using the MetOp Infrared Atmospheric Sounding Interferometer, Atmospheric Measurement Techniques, 4, 1567–1580, https://doi.org/10.5194/amt-4-1567-2011, 2011.

Walker, J., Carboni, E., Dudhia, A., and Grainger, R.: Improved detection of sulphur dioxide in volcanic plumes using satellite-based hyperspectral infrared measurements: Application to the Eyjafjallajökull 2010 eruption, Journal of Geophysical Research: Atmospheres (1984–2012), 117, https://doi.org/10.1029/2011JD016810, 2012.

Watt, S., Mather, T., and Pyle, D.: Vulcanian explosion cycles: Patterns and predictability, Geology, 35, 839–842, https://doi.org/10.1130/G23562A.1, 2007.

Yu, T., Rose, W. I., and Prata, A. J.: Atmospheric correction for satellite-based volcanic ash mapping and retrievals using "split window" IR data from GOES and AVHRR, Journal of Geophysical Research: Atmospheres, 107, AAC 10–1–AAC 10–19, https://doi.org/10.1029/2001JD000706, 2002.

Yue, J., Miller, S. D., Straka III, W. C., Noh, Y.-J., Chou, M.-Y., Kahn, R., and Flower, V.: La Soufriere Volcanic Eruptions Launched Gravity Waves Into Space, Geophysical Research Letters, 49, e2022GL097 952, https://doi.org/10.1029/2022GL097952, 2022.

Zakšek, K., Hort, M., Zaletelj, J., and Langmann, B.: Monitoring volcanic ash cloud top height through simultaneous retrieval of optical data from polar orbiting and geostationary satellites, Atmospheric Chemistry and Physics, 13, 2589–2606, https://doi.org/10.5194/acp-13-2589-2013, 2013.